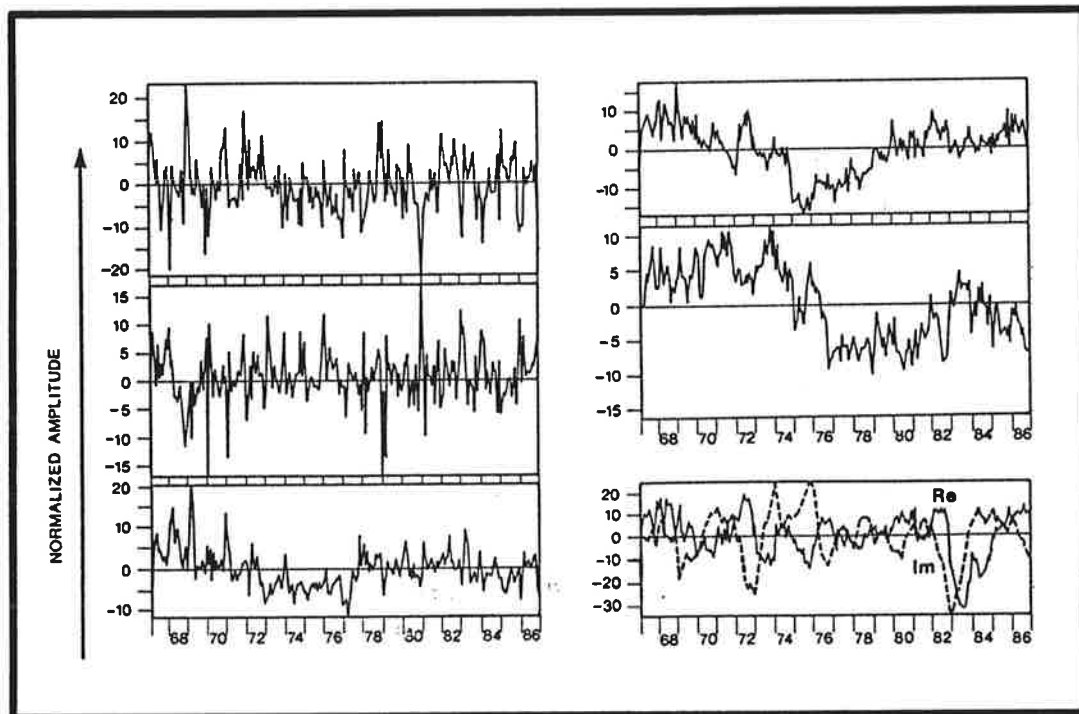




# Max-Planck-Institut für Meteorologie

## REPORT No. 78



### THE JOINT NORMAL MODES OF THE COUPLED ATMOSPHERE—OCEAN SYSTEM OBSERVED FROM 1967 TO 1986

by

JIN—SONG XU

HAMBURG, JANUARY 1992

AUTHOR:

JIN-SONG XU

MAX-PLANCK-INSTITUT  
FÜR METEOROLOGIE

MAX-PLANCK-INSTITUT  
FÜR METEOROLOGIE  
BUNDESSTRASSE 55  
D-2000 HAMBURG 13  
F.R. GERMANY

Tel.: +49 (40) 4 11 73-0  
Telex: 211092 mpime d  
Telemail: MPI.METEOROLOGY  
Telefax: +49 (40) 4 11 73-298

REPb 78

# THE JOINT NORMAL MODES OF THE COUPLED ATMOSPHERE-OCEAN SYSTEM OBSERVED FROM 1967 TO 1986

Jin-Song Xu

Max-Planck-Institut für Meteorologie

January 1992

## ABSTRACT

Two aspects of the Principal Oscillation Pattern (POP) analysis are used to study the joint normal modes of the coupled atmosphere-ocean system from a combined dataset including both atmospheric (sea level pressure, 700-mb and 200-mb zonal wind) and oceanic (sea surface temperature, Pacific sea level and Pacific subsurface temperature) parameters. The first aspect is that the Principal Oscillation Patterns can be considered as normal modes of the analyzed system. Because of the complexity of the coupled system, a straightforward method of studying these normal modes is to estimate them from the data. The second aspect of the POP analysis is that it can be considered as a multivariate spectral analysis. The spectral types of the modes are by-products of the POP analysis.

Six joint normal modes of the coupled atmosphere-ocean system are found in this study. For Mode 1, 2 and 3 whose spectra are white or nearly white, the atmosphere plays an important role. The associated oceanic anomalies seem to be generated by the anomalous atmospheric conditions. For the other modes which have most of their power on much longer time scales, the ocean is more actively involved. Modes 4 and 5 describe decadal time scale variations. Mode 4 is characterized by changes in SST in all three tropical oceans, and in organized convection over the West Pacific. The results allow us to speculate further that these tropical features might excite changes in the extratropical tropospheric and oceanic circulations. Mode 5 shows global scale SST anomalies and large anomalies in the Southern Hemispheric circulation. Mode 6 is the only oscillatory normal mode found in the coupled atmospheric-ocean system, it describes the quasi-cyclic behaviour of the El Niño/Southern Oscillation phenomenon.

## 1. INTRODUCTION

At present, the length of available upper-air atmospheric and subsurface oceanic data records is about 20 to 30 years. These data sets offer a possibility of constructing a more detailed data set for the atmosphere-ocean system. Two kinds of observational studies using (near) global data sets have been done so far. The first kind has been concerned with variability in one or a few of the parameters. The second kind has concentrated on one particular phenomenon, e.g. the El Niño/Southern Oscillation (ENSO). Generally, variability within each data set is well documented and some phenomena, particular those with shorter time scales, are well described. For variations on decadal time scales, although some time series are documented, the spatial distributions of such variations are less-known. There has been no study which systematically considers joint normal modes in a combined data set containing both global atmospheric and oceanic parameters.

The purpose of this paper is to detect and to understand joint modes on time scales of months to years (probably to decades) in the coupled atmosphere-ocean system. For that purpose a combined data set is used, including ocean temperature, sea level, sea surface temperature (SST), sea level pressure (SLP) and low and high level zonal winds. To identify signals within the atmosphere-ocean system, the Principal Oscillation Pattern (POP) analysis is used. The technique was introduced by Hasselmann (1988) and Storch et al. (1988). Its feasibility in capturing the spatial and temporal characteristics of one or two signals in a data set was shown by, among others, Xu and Storch (1990) and Xu (1991). In this paper, the POP analysis is described only briefly. In section 2, two aspects of the POP analysis are emphasized which are crucial for this paper, but were not explicitly used in the earlier studies. In Section 3, some ideas are described which can be used to specify the physical processes involved in each signal. Data and data processing are described in section 4. The joint modes that are found are presented and discussed in section 5. Conclusions are given in section 6.

## 2. IDENTIFYING THE SIGNALS: the POP analysis

### a) POPS AS ESTIMATED NORMAL MODES

The following notations are used: vectors are given in **bold** and matrices in gothic.  $\top$  denotes transpose,  $*$  represents the complex conjugate, and  $\cdot$  indicates dot product.

The POP formalism assumes that an  $m$ -dimensional state vector  $\mathbf{x}(t)$  is modeled by a linear equation:

$$\mathbf{x}(t+1) = \mathfrak{B} \mathbf{x}(t) + \mathbf{n}(t) \quad (1)$$

where  $\mathfrak{B}$  is a constant matrix and  $\mathbf{n}(t)$  represents the noise time series. The eigenvectors of  $\mathfrak{B}$  are called Principal Oscillation Patterns (POPs). Because, in the framework of the POP analysis,  $\mathfrak{B}$  is estimated from data (see e.g. Xu and Storch, 1991), the POPs can therefore be considered as estimated normal modes.

Generally for any dynamical model, the discrete form of linearized equations for disturbances can also be written in the form of the deterministic part of equation (1). Unlike in the POP analysis, in which the system matrix  $\mathfrak{B}$  is estimated from data and depends on the mean state derived from data over a certain period, the system matrix of a linearized theoretical model is determined from physical laws and depends on a pre-specified mean state. Therefore, there is an unambiguous correspondence between the estimated normal modes of data (POPs) and the theoretically-determined normal modes of a physical system. Storch et al. (1991) were able to show that the free atmospheric baroclinic waves can be described both by the POPs and by the most unstable normal modes of a linearized quasi-geostrophic vorticity equation with a zonally-symmetric basic state.

In this paper we are interested in the normal modes of the coupled atmosphere-ocean system. For this purpose, the straightforward approach is to estimate the system matrix and its normal modes from the data, rather than from theoretical equations.

Generally  $\mathfrak{B}$  is not symmetric so that the eigenvectors  $\mathbf{P}$  and their eigenvalues  $\lambda$  are either real or appear in conjugate pairs. The state of  $\mathbf{x}(t)$  may be described by the  $m$  POPs  $\mathbf{P}_j$ :

$$\mathbf{x}(t) = \sum_j^m z_j \mathbf{P}_j \quad (2)$$

- Because eigenvector of a matrix is only defined to an arbitrary factor  $ce^{i\theta}$  (for real eigenvector  $\theta=0$ ), we need to choose some standard normalization for the POPs. In this study,  $c$  is chosen so that the length of (real or imaginary part of) the eigenvector is equal to  $m$ . For a complex POP,  $\theta$  needs also to be specified (see section 5.4).

According to (2), a signal in the form of  $z_j P_j$  has the same unit as in  $x(t)$ , i.e. if  $x(t)$  represents temperature anomalies in °C,  $z_j P_j$  gives temperature anomalies in °C for the considered  $j$ -th signal. This notion is frequently used in section 5.

Because of the linear assumption made in (1), the evolution of coefficients is given by:

$$z_j(t+1) = \lambda_j z_j(t) + n_j(t) \quad (3)$$

where  $n_j(t)$  is related to  $n(t)$ .

#### b) POP ANALYSIS AS MULTIVARIATE SPECTRAL ANALYSIS

Equation (3) can also be translated into the frequency domain. After some manipulations, the auto spectrum  $\Gamma_{z_j}(\omega)$  of the POP coefficient time series  $z_j(t)$  can be written:

$$\Gamma_{z_j}(\omega) = \frac{\Gamma_{n_j}(\omega)}{(e^{i\omega} - \lambda_j)(e^{-i\omega} - \lambda_j^*)} \quad (4a)$$

where  $\Gamma_{n_j}(\omega)$  is the auto spectrum of the noise  $n_j(t)$ . The auto spectrum  $\Gamma_{z_j}(\omega)$  is a function of the noise auto spectrum  $\Gamma_{n_j}(\omega)$  and the eigenvalue  $\lambda_j$ . If the POPs in equation (2) capture all signals in the data  $x(t)$ ,  $\Gamma_{n_j}(\omega)$  should be white or at least smooth. In this study, the noise time series are also calculated (not shown). As expected, they are white. Equation (4a) then presents different types of spectra depending on the magnitude of  $\lambda$  and whether  $\lambda$  is complex or real. In the following  $|\lambda| < 1$  is assumed, which is usually true for stationary time series.

#### Peak Spectrum ( $\lambda$ is complex and $|\lambda| \rightarrow 1$ )

This type of spectrum is obtained when an eigenvalue is complex, i.e.  $\lambda_j = |\lambda_j| e^{i\phi_j}$ . For  $|\lambda_j| = 1$ , a resonance peak occurs at frequency  $\phi_j$ . For  $|\lambda_j| < 1$ , spectrum (4a) exhibits a maximum centered at frequency  $\phi_j$  with width determined by  $|\lambda_j|$ . The smaller  $|\lambda_j|$  is, the broader the maximum is. The eigenvalue determines, therefore, not only the oscillation frequency but also the shape of the spectrum.

For a complex POP  $\mathbf{P} = \mathbf{P}_j^{re} + i\mathbf{P}_j^{im}$ , if  $|\lambda_j|$  is near 1, the signal identified by the POP describes the oscillatory tendency<sup>1</sup> :

$$\begin{array}{ccc}
 & \mathbf{P}_j^{im} & \\
 & \nearrow & \searrow \\
 -\mathbf{P}_j^{re} & & \mathbf{P}_j^{re} \\
 & \nwarrow & \nearrow \\
 & -\mathbf{P}_j^{im} & 
 \end{array} \quad (5)$$

with oscillation period  $T_j=2\pi/\phi_j$  and e-folding time  $= \frac{1}{\ln|\lambda_j|}$ .

Red Noise Spectrum ( $\lambda$  is real and  $\lambda \rightarrow 1$ ) and White Noise Spectrum ( $\lambda \rightarrow 0$ )

In the case of a real eigenvalue, equation (4a) can be rewritten:

$$\Gamma_{z_j}(\omega) = \frac{\Gamma_{n_j}(\omega)}{(1-2\lambda_j \cos\omega + \lambda_j^2)} \quad (4b)$$

which describes a red noise spectrum when  $\lambda_j \rightarrow 1$ , and a white noise spectrum when  $\lambda_j \rightarrow 0$ .

Equations (4a) and (4b) demonstrate that the POP analysis is able to quantify the spectral features of the corresponding pattern by a single number  $\lambda_j$ . Parallel to the conventional univariate spectral analysis, which is used to identify signals in different frequency bands in a 1-dimensional time series, the POP analysis can be considered as a 'multivariate spectral analysis', which isolates multivariate signals, i.e. patterns, across the whole available frequency interval (in this study from 1/(2 month) to 1/(20 years)). In optimal cases, the extensive second moment information in the high dimensional  $\mathbf{x}(t)$  can be compressed into a manageable set of numbers ( $\lambda_j$ ) and patterns (POPs).

<sup>1</sup> Equation (3) describes an anti-clockwise rotation in the 2-dimensional complex-plane. However, for a complex POP, the signal is represented by  $z\mathbf{P} + z^*\mathbf{P}^* = 2z^{re}\mathbf{P}^{re} - 2z^{im}\mathbf{P}^{im}$ , where  $\mathbf{P}^{re}$ ,  $z^{re}$  ( $\mathbf{P}^{im}$  and  $z^{im}$ ) are the real (imaginary) parts of the complex POP and POP coefficient. In practice,  $2z^{re}$  and  $-2z^{im}$  are used to describe the time evolution of signal  $\mathbf{P}$  and  $\mathbf{P}^*$  ( $2z^{re}$  and  $-2z^{im}$  are noted hereafter as the real and imaginary parts of the POP coefficient). Therefore, clockwise rotation as given in (5) is observed.

It is concluded that the POP analysis is not only useful for estimating normal modes of data, but also provides a simple diagnostic tool for expressing the spatial and spectral characteristics of these modes.

### 3. SPECIFYING PHYSICAL PROCESSES

Although the POP analysis provides an easy answer to the question of what the normal modes of the considered system look like, the results of a POP analysis do not suggest what physical mechanism is involved in each mode. For understanding these modes something else has to be done.

The basic idea for specifying physical processes is to specify relationships between well known processes and their corresponding anomaly distributions. The purpose of this section is to demonstrate these relationships in terms of the parameters used. Because joint modes of the coupled atmosphere-ocean system are considered in this study, I concentrate mainly on the air-sea processes. In the following discussion, SST is considered as only one possible forcing for the atmosphere, and sea level and subsurface temperature are treated as indicators of oceanic response to atmospheric forcing. The low and high level atmospheric parameters are used to describe the vertical structure of the atmospheric response to oceanic forcings.

#### a) EXTRATROPICAL SST AND THE OVERLYING ATMOSPHERE

In the extratropics, two kind of SST patterns associated with two different air-sea processes have been observed and documented in the literature.

First, if the atmosphere forces the ocean, it would be expected that in the presence of an anomalous anticyclone over the North Atlantic or North Pacific the SST pattern would show anomalous warming at the anticyclone's western and southern flank and cooling at its eastern and northern flank (see also Fig. 1b in Zorita et al., 1992). It is generally understood that the SST anomalies are produced by the warm marine and cold continental air advection brought about by the anomalous atmospheric circulation. This process was first proposed by Bjerknes (1962) and is supported by a GCM study for the North Pacific (Luksch and Storch, 1992). Because the warm marine and cold continental air advection is strongest during the winter time, the above mentioned air-sea process is strongest during the winter time.



In the second case, if the ocean forces the atmosphere, it would be expected that downstream of the positive SST anomalies the low level atmosphere would become warmer and wetter, and negative SLP anomalies would be observed east of the SST anomalies (see also Fig. 1a in Zorita et al., 1992). This process, in which anomalous heating is balanced by horizontal advection of temperature, was proposed by Egger (1977) and Webster (1981).

#### b) TROPICAL SST AND THE OVERLYING ATMOSPHERE

In the tropics, anomalous heating is generally associated with an air-sea interaction process with positive feedback. The atmospheric response to a local heating involves large scale convection over the heating area as already indicated by a simple model (Gill, 1980). The atmospheric anomalies in turn favour the SST anomalies, so that more SST anomalies can be produced.

It is noted that, in the above mentioned pattern of tropical air-sea interaction processes, only local heating anomalies are considered. It is not clear for instance, how the atmosphere would react if the whole tropics were warmer.

#### c) SEA LEVEL AND THE OVERLYING ATMOSPHERE

If slow processes (changes in the shape of the ocean, or land uplift or sinking) are neglected, sea level variation  $\mu'$  can be produced by three processes (Gill and Niiler, 1973):

$$\mu' = \mu'_a + \mu'_s + \mu'_m \quad (6)$$

The first term on the right hand side  $\mu'_a$  is a direct local sea level response to the atmospheric pressure anomalies, known as the inverse barometric effect. An increase of atmospheric pressure  $P_a$  of 1 mbar produces a 1 cm depression of the sea level.

The second term  $\mu'_s$  describes sea level changes caused by changes in the density of the column which imply an expansion or contraction of the column. Because of the strong relation between  $\mu'_s$  and heat and fresh water fluxes which are not available for this study, the second term in equation (6) is not considered in this study.

The  $\mu'_m$  term describes the sea level changes associated with motions in the

upper layers of the ocean. In this study, only wind driving motions are considered. In the oceanic interior, upper layer motions are generally induced by wind forcing via the Sverdrup relation, which fails in the western boundary and equatorial regions. In this paper it is assumed that changes in the western boundary current can be implicitly derived from interior flow changes, i.e. an anomalous southward (northward) interior flow is associated with anomalous northward (southward) return flow on the western boundary. On the Equator, other effects such as Ekman flux (pumping) or equatorial waves become dominant for sea level changes.

Except on the Equator, the sea level anomalies  $\mu'_m$  are related to current anomalies via the geostrophic relation.

The barometric  $\mu'_a$  is mainly forced *locally* by the atmospheric pressure. On the other hand, the response of sea level to motions is *not local* and, in the presence of large scale wind stress curl anomalies, it can be even basin wide.

#### d) OCEANIC RESPONSE IN THE UPPER 200 METERS

Different vertical structure of oceanic anomalies can be produced by changes in the structure of the mixed layer and the thermocline, and by reaction of the ocean in term of barotropic and baroclinic modes. Although subsurface temperatures are used in this study, they are not sufficient for determining these physical processes. Therefore, no further attempt is made to clarify causes of vertical structure of oceanic anomalies.

The summarized air-sea processes and their anomaly distributions are used in section 5 as a guide for understanding the joint modes of the atmosphere-ocean system.

#### 4. DATA

The data used in this paper are monthly anomalies of:

i) The four degree latitude by ten degree longitude SST from the Comprehensive Ocean-Atmospheric Data Set (COADS, Woodruff et al., 1987) prepared by P. Wright (Wright et al., 1988).

ii) The five degree latitude by ten degree longitude temperature in the Pacific Ocean at 10, 50, 125, and 200 meter depth archived at Far Seas

Fisheries Research Laboratory in Japan and at the Scripps Institution of Oceanography in the U.S.A. This data are derived from  $1^0 \times 1^0$  XBT measurements taken at 12 levels and between the surface and about 250 meters. The original bi-monthly data are interpreted into monthly data via a simple time average procedure. In this paper, i) and ii) are used to form a data set for ocean temperature.

iii) Sea level station data in the Pacific collected by Wyrski et al. (1988).

iv) A combined data set of SLP including the Northern Hemisphere SLP ( $20^0\text{N}$ - $50^0\text{N}$ ) stored at the National Center for Atmospheric Research (Boulder, USA), Southern Hemisphere SLP ( $10^0\text{S}$ - $40^0\text{S}$ ) generated at the Bureau of Meteorology Research Center (Melbourne, Australia) and the tropical ( $20^0\text{N}$ - $20^0\text{S}$ ) COADS SLP (Wright et al., 1988).

v) Zonal winds at 200 mb and 700 mb from the National Meteorological Center analysis (Washington DC, USA), which are longitudinally smoothed resulting in a ten degree zonal resolution. The north-south resolution is unchanged with a meridional resolution of about  $3.5^0$  at  $40^0$ , and  $5^0$  in the equatorial region.

The spatial dimension of each data set considered in this paper is of the order of  $10^2$  to  $10^3$ . The order of the system matrix  $\mathcal{B}$  in equation (1) for the combined data set would then be  $10^3$ . To simplify the interpretation of  $10^3$  POPs and to concentrate on the large scale variations, each data set is compressed into the smaller space spanned by the first few EOFs. No effort is made to check the significance of the EOFs. Because the error in estimating the lower order EOFs is much larger than that of the higher order EOFs, only EOFs that explain more than 1% of the total variance are used in this study. The data information and results of the data compression are shown in Table 1.

The dimension of the combined system  $x(t)$  is then 95. In this paper the variances of the oceanic and atmospheric data are adjusted so that they are equal. It is noted that, because more data are available in the Pacific region, variability in that region might be emphasized. The 95-dimensional combined system is further compressed into the space spanned by the first 9 EOFs of this system. These EOFs, which are the input vector time series  $x(t)$  for the POP analysis, explain 56% of the variance of the combined data set and about 45% of the original data set. The results obtained within the 9-dimensional space are then translated back into the physical space.

TABLE 1: Informations of dimensions of the datasets, numbers of EOFs used for the combined dataset and variance explained by these EOFs for each data set.

data sets used	dimensions of the original data sets	no. of EOF used for the combined data set	variance explained by these EOFs
i & ii	1061	25	71%
iii	79	21	92%
iv	1331	23	81%
v	1656	26	76%
sum	4127	95	80% (averaged)

TABLE 2: Eigenvalue of each POP and standard deviation  $\delta$  of each POP coefficient time series. For the complex Mode 6, standard deviations of the real and imaginary part of the coefficient are shown. The standard deviations  $\delta$  are used in section 5 to estimate the averaged strength of each mode.

	$\lambda_j$	standard deviation $\delta_j$
Mode 1	0.15	0.05
Mode 2	0.40	0.09
Mode 3	0.66	0.05
Mode 4	0.86	0.07
Mode 5	0.92	0.06
Mode 6	$0.93 e^{i2\pi/51}$	0.11 / 0.10

The EOF compression from a dimension of 4127 for the original data sets to 95 for the combined data set and to 9 for a subspace of the combined data set can be interpreted as a two-step spatial filter: in the first step from a dimension of 4127 to 95, small scale variations within *each* data set are compressed, and in the second step from a dimension of 95 to 9, small scale variations within the *combined* data set are compressed. Therefore, the POPs identified from spatially filtered data are likely large-scale joint modes of the coupled air-sea system.

Because data sets i) and v) begin in 1967 and 1968, and iii) in 1975, and most of the data sets end in 1986, the time period of the combined data set is chosen to be 1967 to 1986. In order to study the variability of the combined data set across the whole available frequency interval, *no time filter* is performed.

Rather than filling missing data by interpolation, the missing data are ignored in the EOF and POP calculation. Thus each matrix element is estimated individually. The principal components  $\alpha_i(t)$  for EOF  $e_i$  are estimated according to a least squares fit by

$$\alpha_i(t) = \frac{\mathbf{e}_i^T \cdot \mathbf{x}(t)}{\mathbf{e}_i^T \cdot \mathbf{e}_i} \quad (7)$$

## 5. RESULTS

In the 9-dimensional subspace, two complex POPs together with their complex conjugates and 5 real POPs are found. One of the complex POPs has eigenvalue  $\lambda=0.5 e^{i2\pi/103}$ , but the coefficient time series has most of its power at a frequency much higher than  $1/(103 \text{ months})$ . Thus equation (5) is not a valid interpretation. We consider this POP to be "meaningless", and it is not considered in the following discussion. The eigenvalues of the other 6 POPs are listed in Table 2.

The eigenvalues indicate two white spectra with  $|\lambda_{1,2}|=0.15, 0.4$ , and one spectrum with  $\lambda_3=0.66$  which is not purely white or red, two red spectra with  $|\lambda_{4,5}|=0.86, 0.92$ , and one peak spectrum with spectrum maximum around 51 months and an e-folding time of about 12 months. Fig.1 and Fig.2 show the POP coefficient time series and the spectra derived from the time series. As expected, both Fig.1 and Fig.2 confirm the spectrum types suggested by the eigenvalues. The oscillation period for the complex POP is about 40 months in Fig. 2f and is, therefore, overestimated by the complex eigenvalue.

To test the stability of the results, the POP analysis is also performed using different numbers of EOFs. It turns out that in all these cases only 6 POPs are interpretable, the others appear as "meaningless" POPs. In the following I will concentrate on the 6 signals  $P_j$  ( $j=1,\dots,6$ ) identified by the five real POP and one complex POP listed in Table 2.

In this section, two diagrams are usually shown for each POP, one for the atmospheric part of a POP (SLP, 700-mb and 200-mb zonal wind) and the second for the oceanic part of a POP (SST, Pacific subsurface temperature and sea level). For some of the signals, one or two parameters are not shown. In this case the variability in the missing variable is negligible or irrelevant for the considered mode, and therefore not presented.

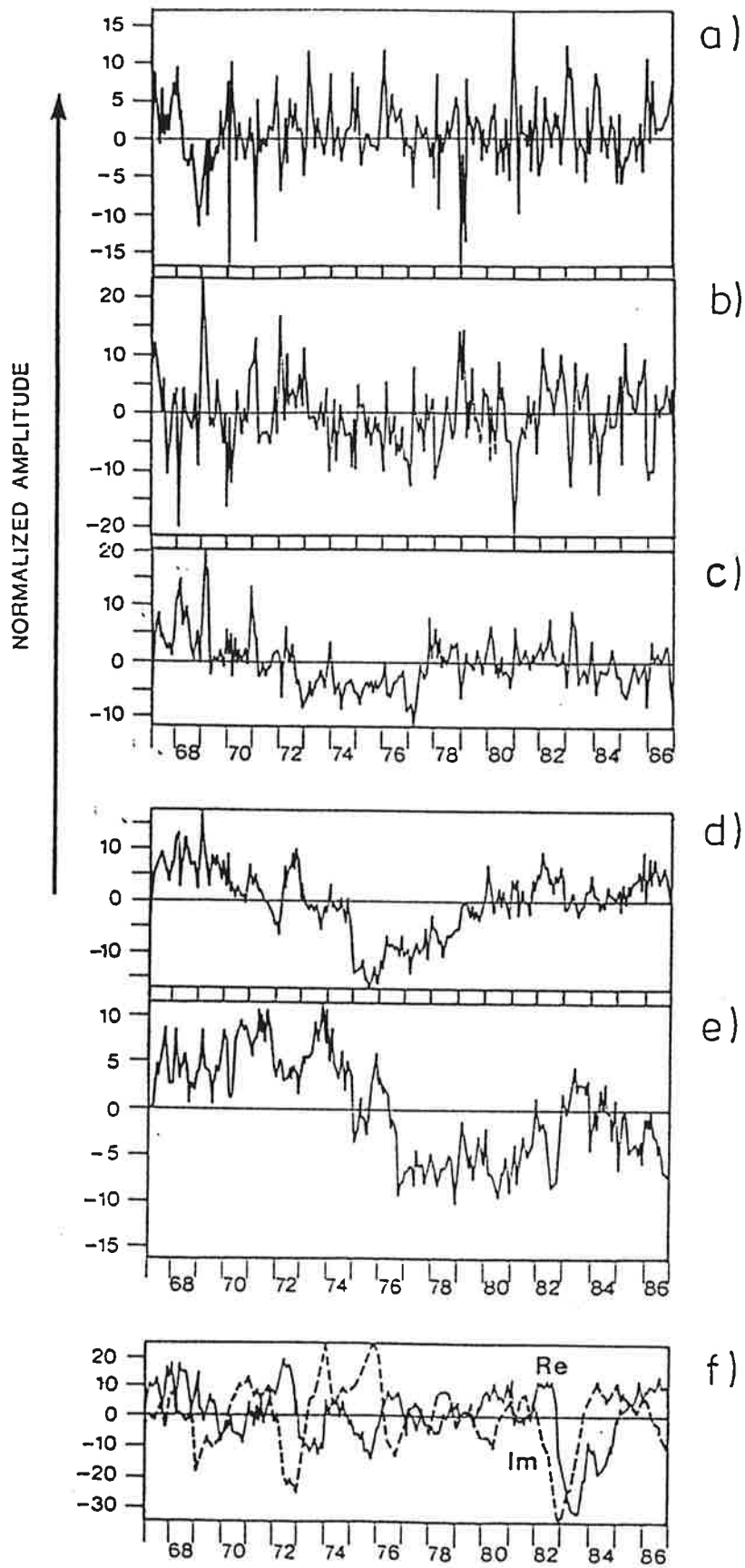


Figure 1: POP coefficient time series of Mode 1 to Mode 6 as listed in Table 2.

AUTOSPECTRUM

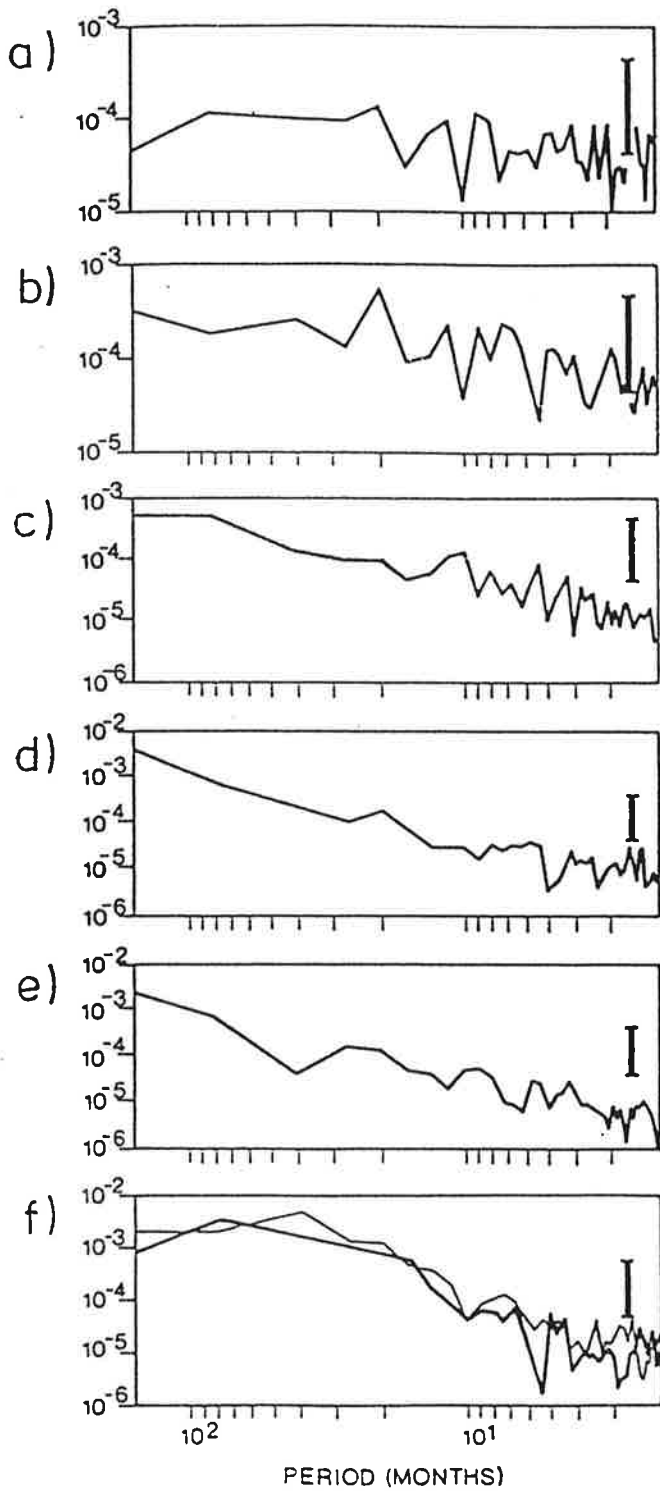
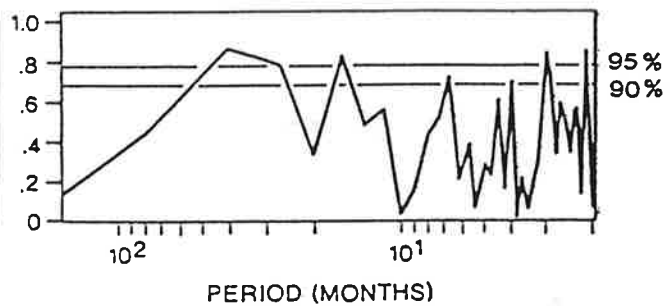


Figure 2: Spectra estimated from the POP coefficient time series for Mode 1 to Mode 6. For the complex Mode 6, both auto spectrum and the coherence spectrum of the imaginary and real part of the complex POP coefficient are shown. The vertical bar indicates the uncertainty range at 95% confidence level.

SQUARED COHERENCY SPECTRUM



## 5.1 JOINT NORMAL MODES: Mode 1, Mode 2 and Mode 3

As will be shown shortly, the three modes with smaller eigenvalues (Table 2 and Fig. 2a, 2b, 2c) have many features in common. For this reason they are considered together in this section.

### a) CENTERS OF ACTION

The centers of action of each mode can be identified by the regions of large explained variance which are shaded in Fig.3, Fig.5 and Fig.7. All three modes are confined to the Northern Hemisphere: Mode 1 in the North Atlantic (Fig.3), Mode 2 in the North Pacific (Fig.5), and Mode 3 in the region from the central North Pacific to the North Atlantic (Fig. 7).

Although the wind field and the SLP field extend only to about 50°N, Fig.3, 5, and 7 bear strong resemblance respectively to the "Pacific/North America" (PNA), "East Atlantic" (EA) and "West Atlantic" (WA) teleconnection patterns noted by Wallace and Gutzler (1981). Similar to EA and WA, Mode 1 and Mode 3 describe north-south seesaws over the North Atlantic with the seesaw center in the Mode 1 being shifted southeastward relative to that in Mode 3.

For each mode, the POP patterns for 700-mb and 200-mb zonal wind are nearly identical (not shown). It indicates that these modes are barotropic.

### b) SEASONAL DEPENDENCE

All three of these modes show strong seasonal dependence. Fig.9 gives a frequency distribution of the 3 POP coefficients larger than one standard deviation in each calendar month. It turns out that strong positive and negative amplitudes of these modes occur mostly during the winter season.

### c) THE ROLE OF ANOMALOUS WARM AND COLD AIR ADVECTION

For Mode 2, positive SLP (Fig.5) and easterly anomalies (not shown) are found in the North Pacific, equivalent to an anomalous anticyclone over that region. The SST anomalies shown in Fig.6a are positive over the North Pacific near 40°N, i.e. at the western and southern flanks of the anticyclone which is indicated by the arrow, and negative in the east North Pacific and along the North American coast, i.e. at the anticyclone's eastern and northern flank. Considering the seasonal dependence of this mode, the spatial distributions of



SST anomalies fit perfectly to the process associated with warm and cold air advection, rather than the process proposed by Egger and Webster.

For Mode 1 and 3, the role of anomalous warm and cold air advection, as indicated by the arrows in Fig. 4 and 8, can also be identified.

The results suggest that the anomalous heat fluxes associated with the anomalous warm and cold air advection control the large scale SST changes for all three modes. The maxima of variance explained by these modes are about 20% for the atmospheric parameters and about 5-10% for the oceanic parameters.

#### d) INVERSE BAROMETRIC EFFECT

In Mode 2, large sea level anomalies (Fig.6b) are found directly below the anomalous anticyclone in Fig.5. The maximal pressure anomaly given by  $z_2 P_2$  is about 9 mb (with  $z_2 =$  one standard deviation  $\delta_2=0.09$ , and  $P_2=100\text{mb}$ ), which is roughly balanced by the largest sea level anomaly of about -11cm (with  $z_2=\delta_2=0.09$ ,  $P_2=-1219$  mm). The inverse barometric effect seems to be the dominant effect for sea level anomalies shown in Fig.6b. For the Modes 1 and 3, no sea level data are available over the Atlantic.

#### e) ORIGIN OF THE SIGNALS

In a theoretical normal modes study, Simmons et al. (1983) suggested that the origin of the teleconnection patterns lies in the atmosphere. Consistent with their suggestion, our study shows further the way how the atmospheric and oceanic anomalies of these modes are related to each other. According to such relationship, we conclude that this is the internal dynamics of the atmosphere which generates the patterns shown in Fig.3, 5 and 7, and the ocean acts only passively.

Because the teleconnection patterns vary on month to month time scales (Simmons et al., 1983) and the oceanic reaction time to the atmospheric pressure anomalies and the anomalous warm and cold advection is short (shorter than one month), we suggest that for mode 3 which does not have a purely white noise spectrum, there must be some other processes which generate the low frequent part of the mode.

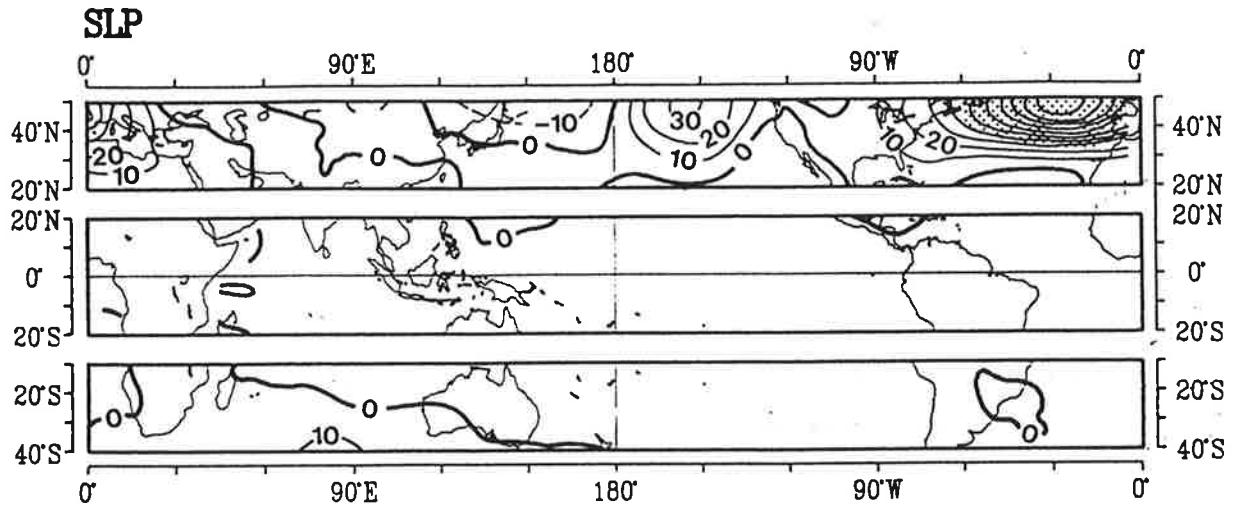


Figure 3: POP pattern of Mode 1 for the sea level pressure (in mb). Shaded area indicates explained variance larger than 20%.

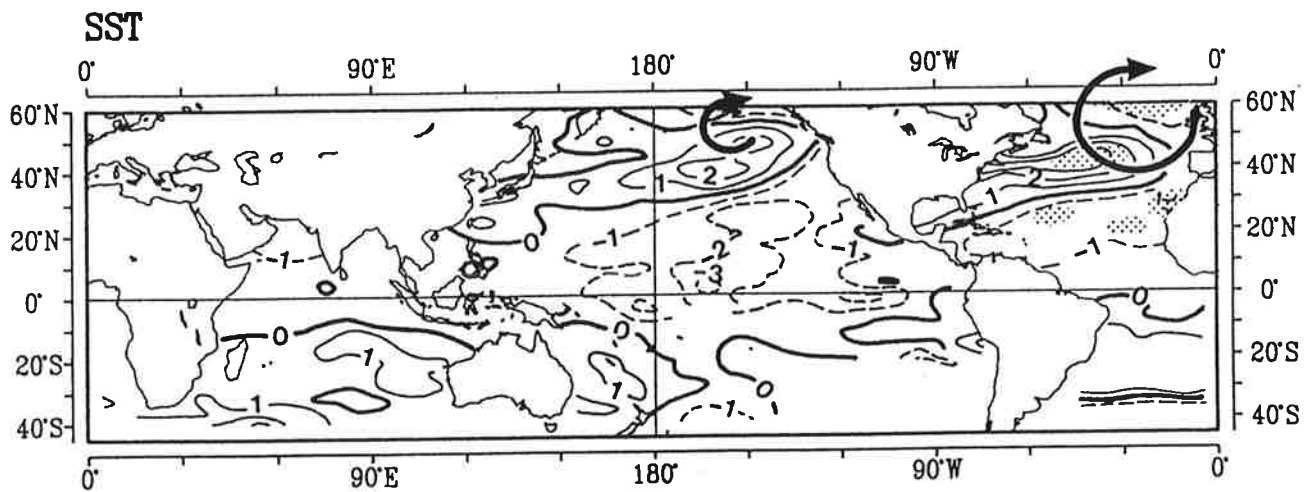


Figure 4: POP pattern of Mode 1 for sea surface temperature (in °C). Shaded areas indicate explained variance larger than 3%.

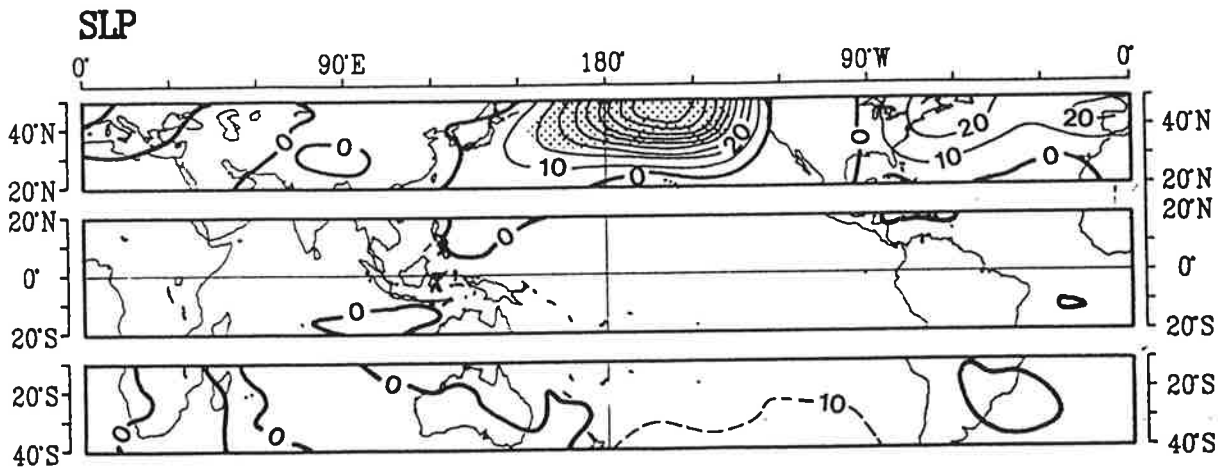


Figure 5: POP pattern of Mode 2 for the sea level pressure (in mb). Shaded area indicates explained variance larger than 20%.

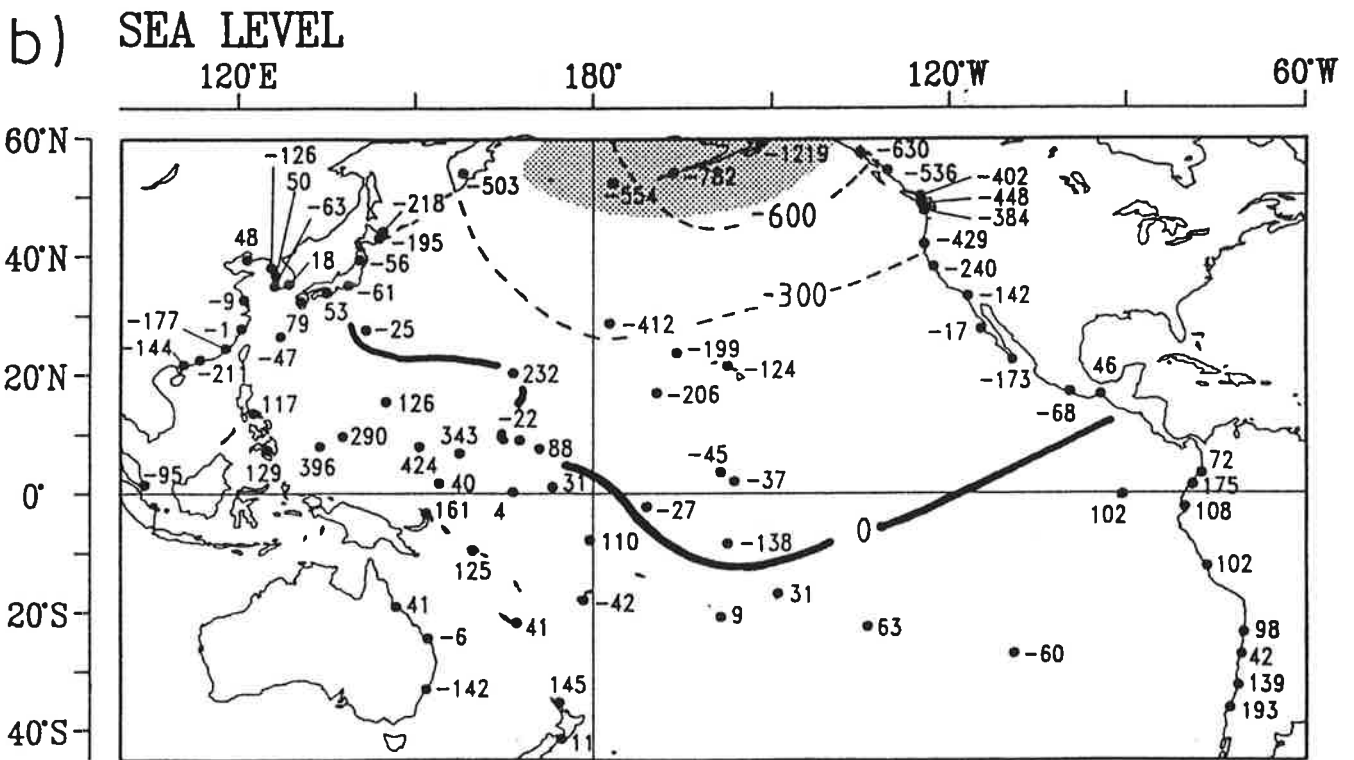
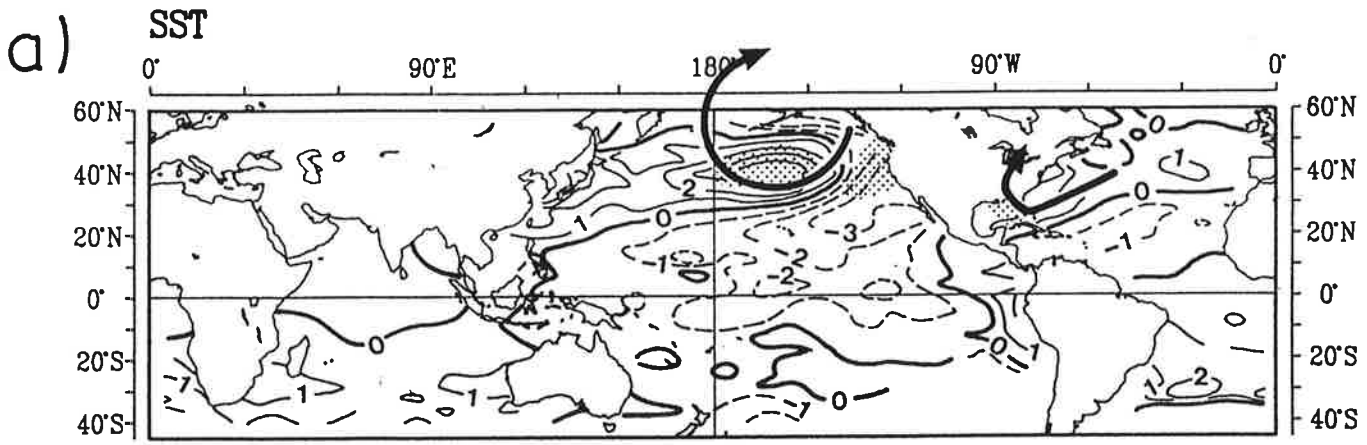


Figure 6: POP pattern of Mode 2 for a) sea surface temperature (in °C), and b) sea level (in mm). Shaded areas indicate explained variance larger than 5% for SST and 10% for sea level.

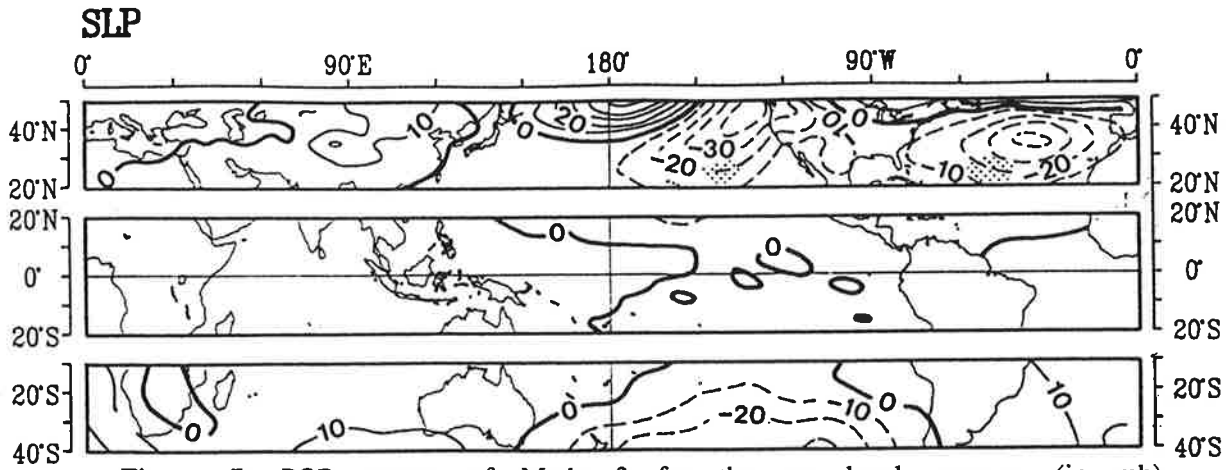


Figure 7: POP pattern of Mode 3 for the sea level pressure (in mb). Shaded areas indicate explained variance larger than 20%.

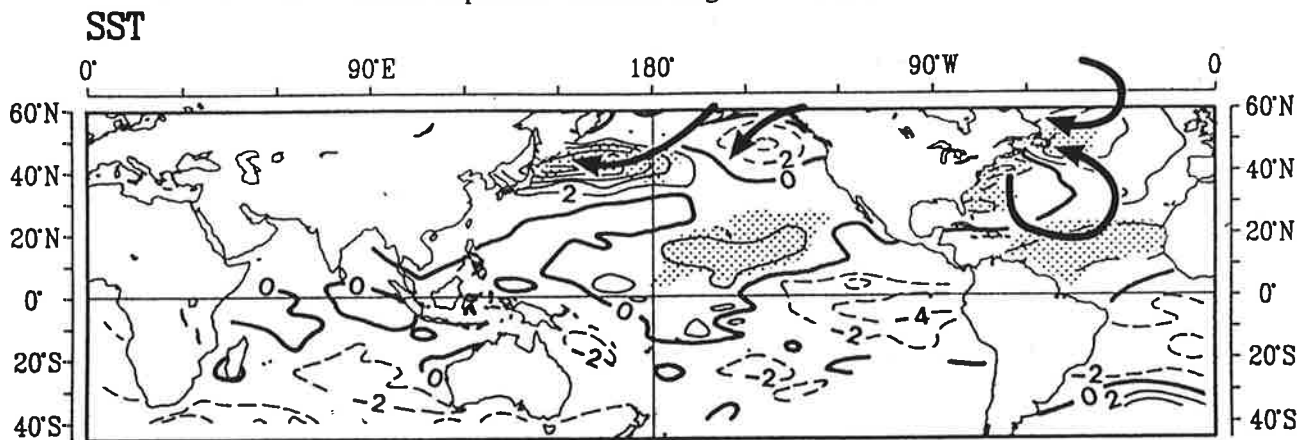


Figure 8: POP pattern of Mode 3 for sea surface temperature (in °C). Shaded areas indicate explained variance larger than 5%.

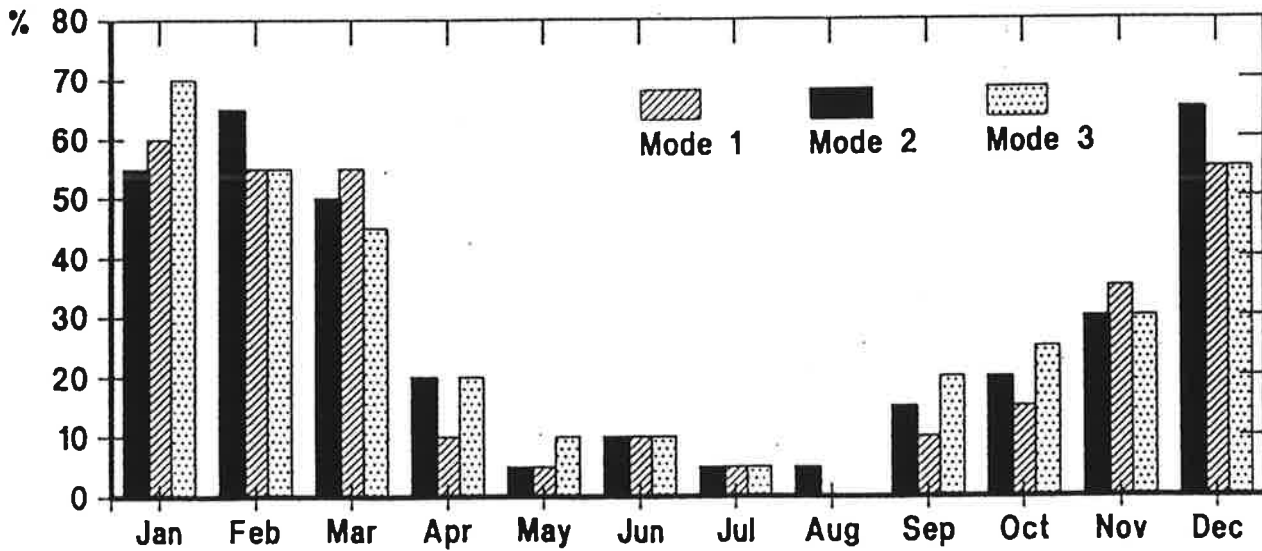


Figure 9: Frequency distribution of POP coefficients larger than one standard deviation for each calendar month.

## 5.2 THE JOINT NORMAL MODE ON DECADEAL TIME SCALES: Mode 4

### a) TROPICAL FEATURES

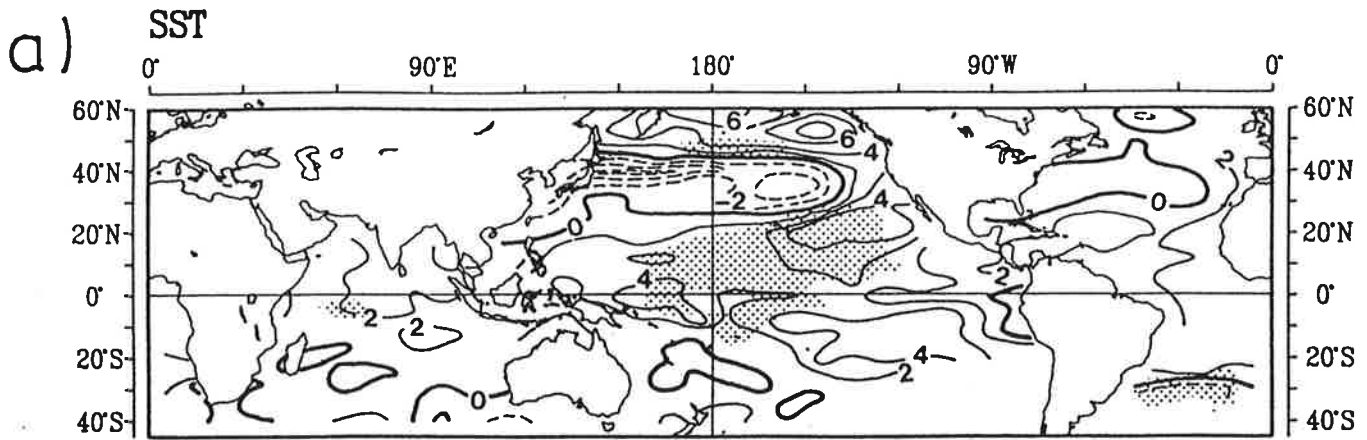
The most striking features of this mode are the large positive SST anomalies in all tropical oceans (Fig.10a) with maximum SST values in the western Pacific on the Equator and in the subtropical Pacific and weak anomalies along the Equator in the eastern Pacific. The coefficient time series of this mode (Fig.2d) indicates variation on a decadal time scale. The increase of the amplitude of the POP coefficient time series since 1975 together with the positive sign of SST anomalies describes a pronounced increase of SST in the global tropical ocean up to several tenth C°.

In the atmosphere, in view of the evidence that SSTs in excess of approximately 28°C are required to support organized convection and the fact that the SST anomalies of this mode have rather small amplitude, the convection induced by this mode is expected to be found only over the Indonesian region and the East Pacific where, in the climatological mean, SSTs of about 28-29°C exist. Indeed, the most pronounced atmospheric feature in the tropics (Fig.11) is the anomalous convergent (divergent) flow over the Indonesian region and the West Pacific at 700-mb (200-mb) as indicated by the westerly (easterly) anomalies over the Indian Ocean and the easterly (westerly) anomalies over the Pacific in Fig.11a (Fig.11b). These patterns lead to the suggestion that the tropical atmosphere does respond to small amplitude variations of the tropical SST forcing (up to a few tenth °C) and displays organized convection centered over the Indonesian region and the West Pacific. Fig.2d indicates further that this convective motion has increased since the mid-seventies.

For the upper layer of the tropical Pacific, Fig.10b shows out-of-phase anomalies with positive values in the first 50 meters and negative values in the layers below in the West Pacific. This vertical structure is different form that observed during ENSO (Fig.17b).

### b) EXTRATROPICAL FEATURES

The largest extratropical atmospheric anomalies are the anomalous westerlies over the central North Pacific and anomalous easterlies over the northern North Pacific at both 700-mb and 200-mb (Fig.11). It is noted that the explained variance for the North Pacific zonal wind is not located in the



b) SUBSURFACE TEMPERATURE

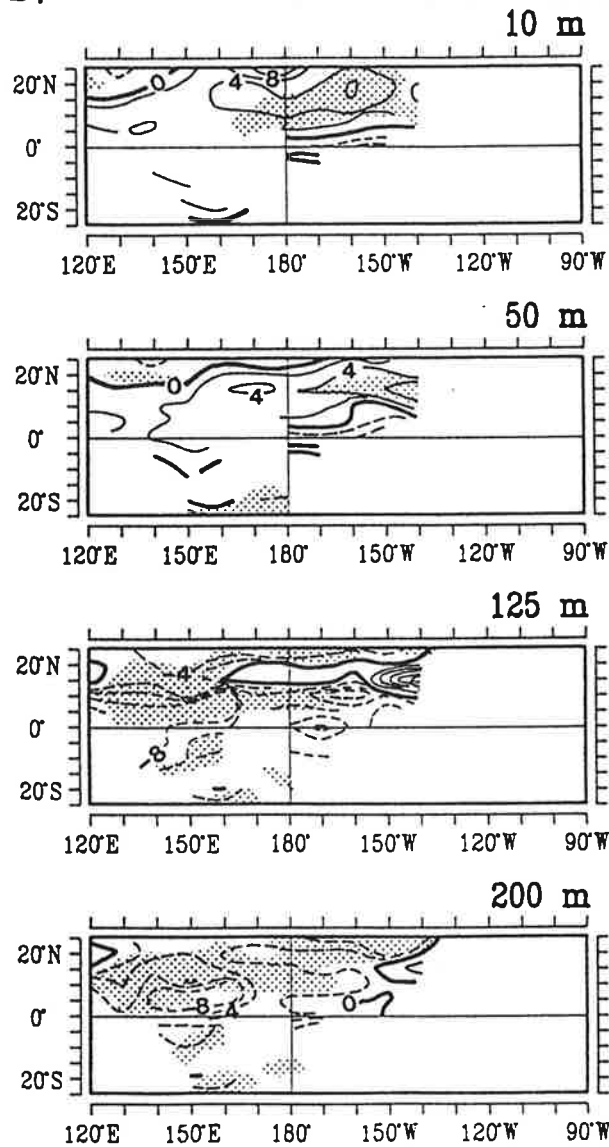
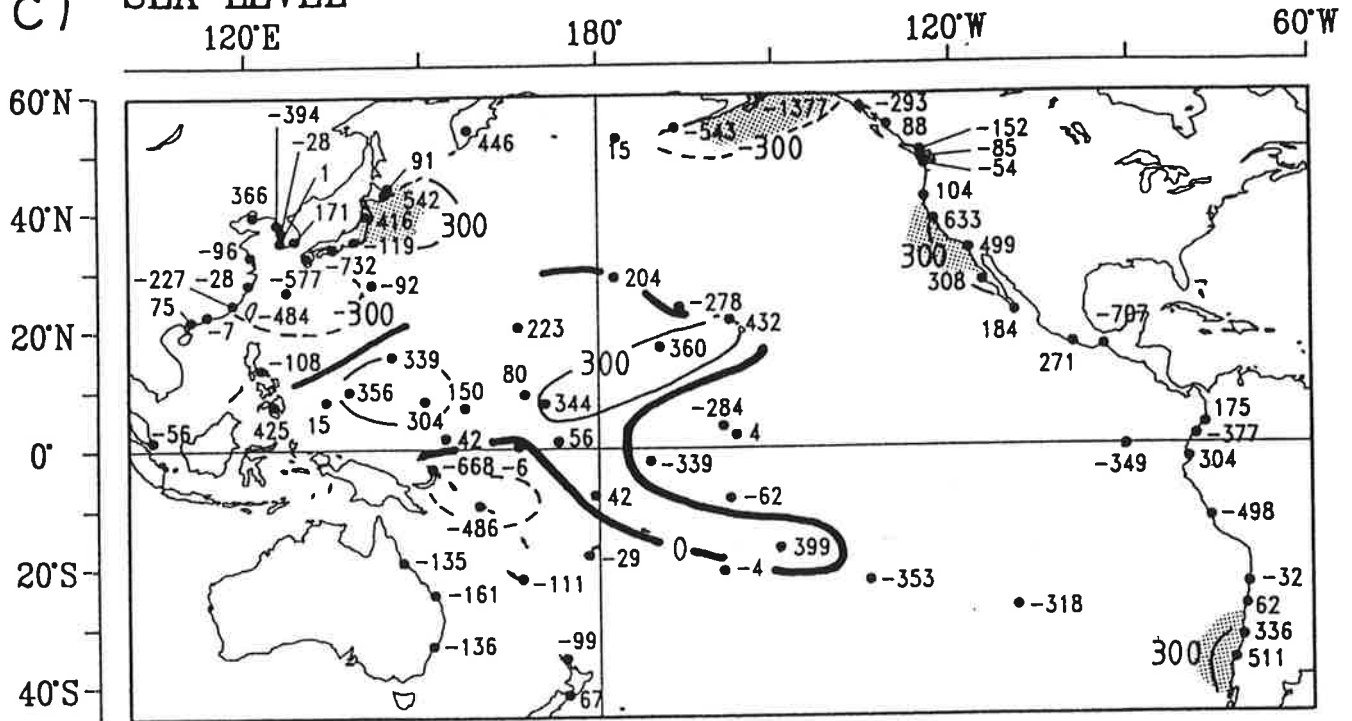


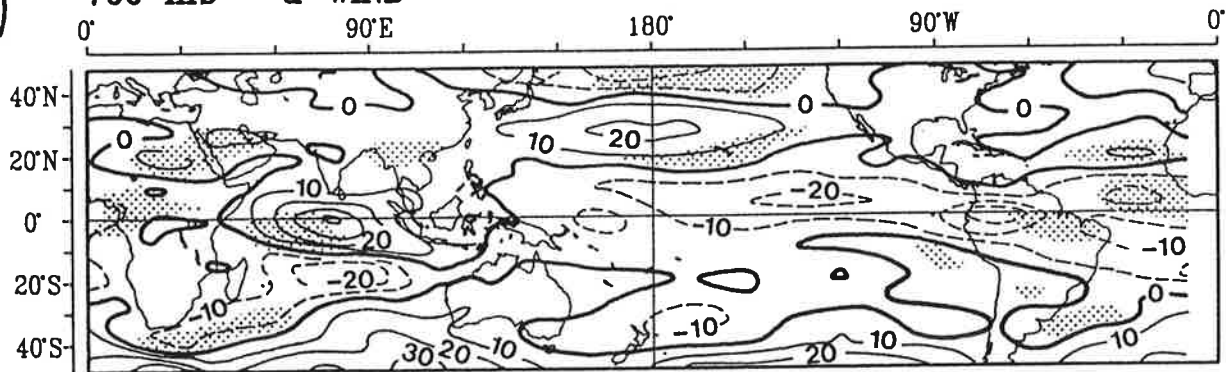
Figure 10: POP pattern of Mode 4 for a) SST (in °C), b) the Pacific sub-surface temperature (°C), and c) Pacific sea level (in mm). Shaded areas indicate explained variance larger than 5% for temperature and 10% for sea level.

c) SEA LEVEL



Continue of Figure 10

a) 700 mb u-WIND



b) 200 mb u-WIND

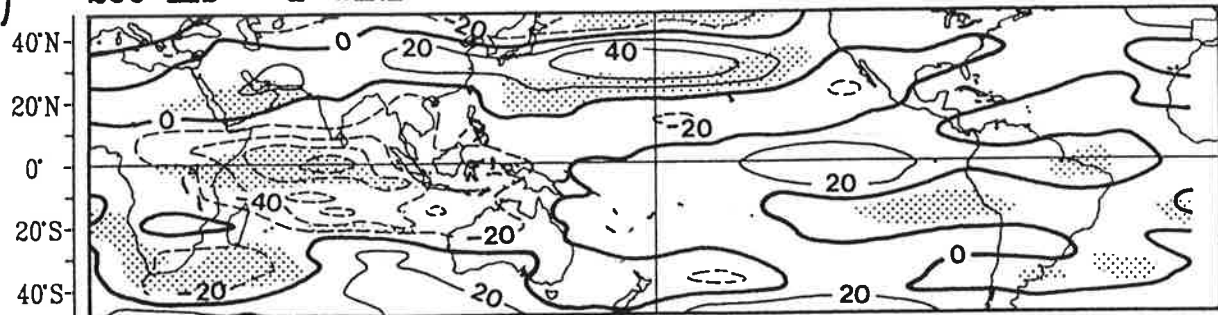
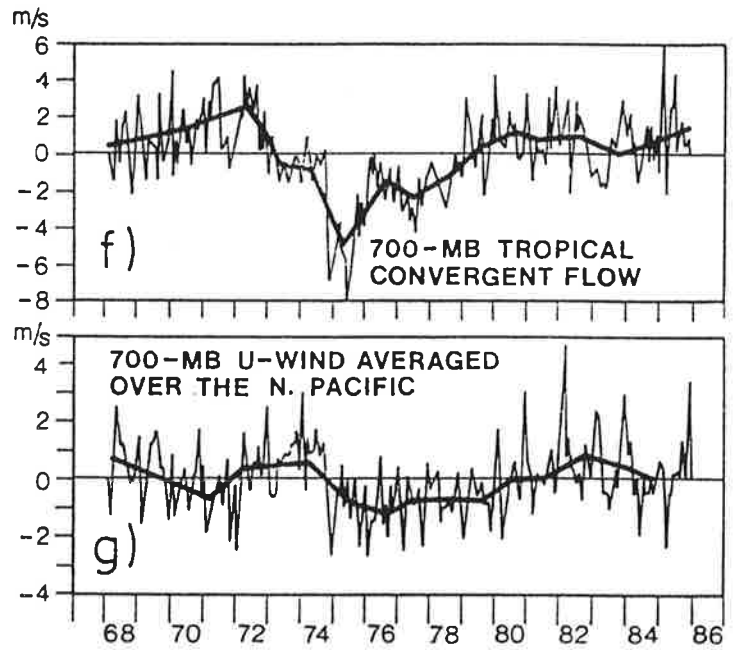
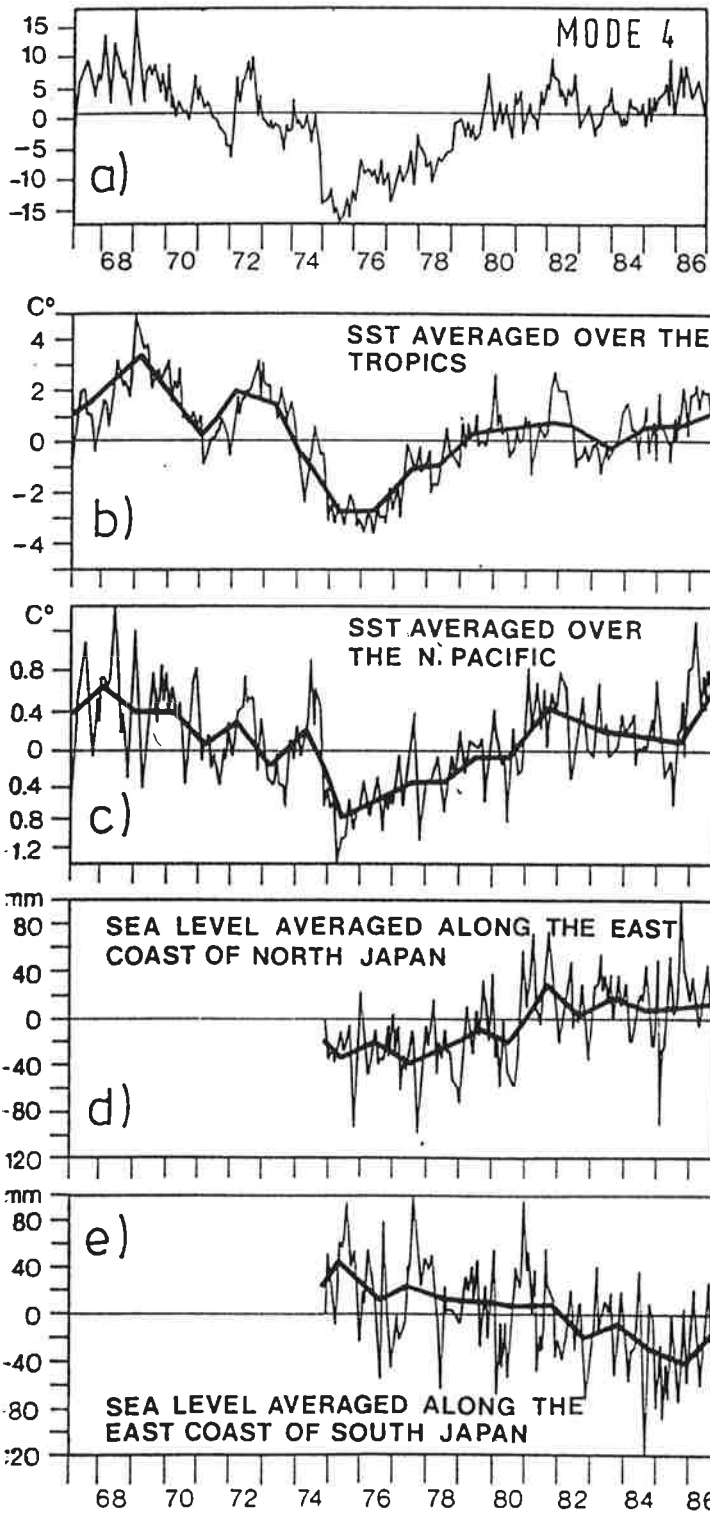


Figure 11: POP pattern of Mode 4 for a) 700-mb zonal wind (in m/s) and b) 200-mb zonal wind (in m/s). Shaded areas indicate explained variance larger than 5%.



**Figure 12:** a) POP coefficient time series of Mode 4, b) global tropical SST averaged over the area from 20°N to 20°S, c) the North Pacific SST which is the difference between area averaged SST in the northern North Pacific (60°N - 44°N) and the central North Pacific (32°N - 40°N), d) sea level anomalies averaged along the east coast of North Japan, e) sea level anomalies averaged along the east coast of South Japan, f) the tropical convergent flow indicated by the difference between zonal wind anomalies over the Indian Ocean and these over the Pacific, g) zonal wind anomalies over the central North Pacific (20°N - 37°N). Units for temperature is °C, for sea level mm and for zonal wind m/s.



regions of anomaly maximum.

In the ocean, large SST anomalies with large negative values zonally orientated along  $40^{\circ}\text{N}$  and large sea level anomalies in the coastal regions are found (Fig.10a,c). Certainly the sea level distribution is affected by the scarcity of data in the oceanic interior. Nevertheless, there are interesting patterns along the coast of Japan with negative anomalies in the South and positive anomalies in the North.

Is it possible that these atmospheric and oceanic changes are related to each other? The wind stress ( $\tau$ ) curl calculated from Fig.11a shows a zero line of curl $\tau$  along  $30^{\circ}\text{N}$  which is located several degrees south of its climatological position (not shown). According to the Sverdrup relation, anomalous circulation induced by zonal wind patterns such as that shown in Fig.11a should have anomalous southward (northward) Sverdrup transport south (north) of  $30^{\circ}\text{N}$ , which in turn might generate northward (southward) return flow along the western boundary. The negative (positive) sea level anomalies along the East coast of southern (northern) Japan (Fig.10c) are consistent with such changes in the Kuroshio and Oyashio Currents. Furthermore, the southward displacement of the zero line of curl $\tau$  indicates a southward displacement of the water mass associated with this current system. The meridional displacement of the water mass might be related to the zonally-orientated SST anomalies along  $40^{\circ}\text{N}$ . The time evolution (Fig.2d) suggests that the Kuroshio and the Oyashio Currents have become stronger since the mid-seventies. This decadal trend in the Kuroshio transport has also been noted by Qui and Joyce (1991).

The above discussion suggests that the extratropical oceanic anomalies which might be described by changes in the strength and the north-southward displacement of the subtropical and subpolar gyres in the North Pacific might be induced by wind changes over that area. However, to prove this idea, more data, especially more compact wind and sea level data, are needed.

In order to ensure that Mode 4 is not an artifact of the analysis technique, area averaged time series which characterize the features described above are calculated. By doing so, other signals in the form of  $z_j P_j$  ( $j=1,2,3,5,6$ ) are subtracted from the original unfiltered anomaly fields.

Fig.12 shows (a) once again the POP coefficient time series, (b) global tropical SST averaged over the area from  $20^{\circ}\text{N}$  to  $20^{\circ}\text{S}$ , (c) the North Pacific

SST which is the difference between area averaged SST in the northern North Pacific (60°N-44°N) and in the central North Pacific (32°N-40°N), (d) sea level averaged along the East coast of northern Japan, (e) sea level averaged along the East coast of southern Japan, (f) the convective flow indicated by the difference between zonal wind anomalies over the Indian Ocean and these over the Pacific, and (g) zonal wind anomalies over the central North Pacific (20°N-37°N).

It is obvious from Fig.12 that the tropical and extratropical features described above indeed develop parallel to each other. The strength of the signal is of order of tenth °C for temperature, a few cm for sea level and a few m/s for zonal winds, as given by  $z_4 P_4$ .

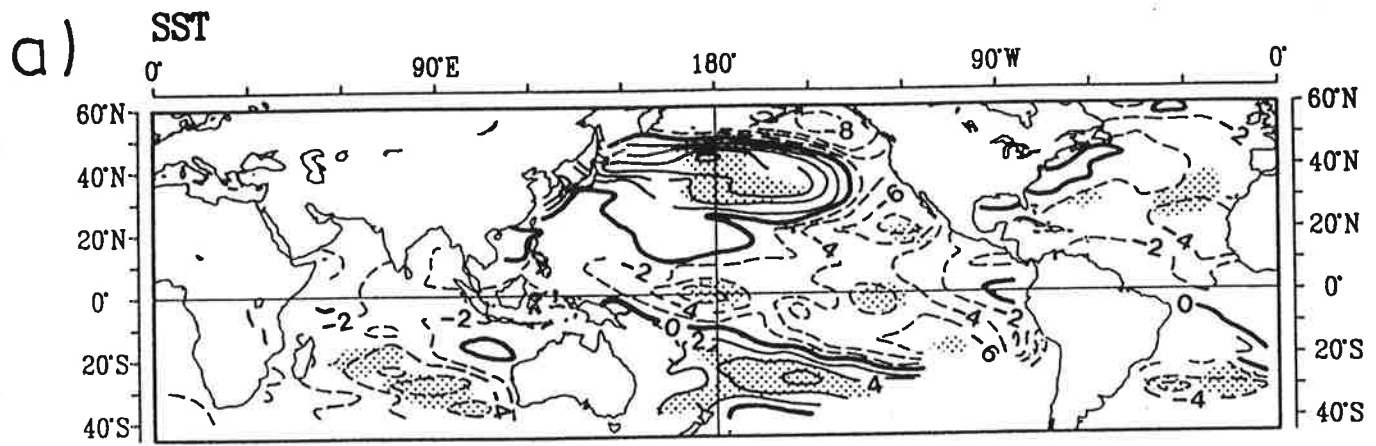
The relationship between the convective changes in the tropics and changes in the extratropical tropospheric circulation has been proposed by Flohn et al. (1990). However, the results shown in this section suggest a more detailed and complex picture of such relationship.

### 5.3 THE JOINT NORMAL MODE ON DECADAL TIME SCALES: Mode 5

The time series of Mode 5 shown in Fig.2e reveals a rather sharp jump during 1975/76. The pattern shown in Fig. 13a indicates that Mode 5 is connected with large-scale SST changes, namely negative anomalies in most parts of the Atlantic and the Indian Ocean, and out-of-phase structure in the Pacific which has negative values in the tropics and positive values in the subtropics. In contrast to Mode 4, where large explained variance is confined to the Pacific, Mode 5 shows large explained variance in SST in all three oceans (shaded areas in Fig. 13a).

The vertical structure of oceanic anomalies, indicated by the subsurface temperature in Fig.13b, resembles that of Mode 4. No signal (in terms of explained variance) is found in sea level.

For the atmospheric parameter, maxima of anomalies and explained variance are found mostly in the Southern Hemisphere at both 700 and 200 mb (Fig. 14a,b). In the tropics, a large-scale organized convection pattern is not observed. In the Southern Hemisphere, easterly anomalies are found over the southern oceans except for a small area in the western South Pacific near 40°S. The mean Southern Hemispheric winter circulation as described by van Loon (1972) is characterized by a strong westerly jet along 45°-50°S with maximum values over



b) SUBSURFACE TEMPERATURE

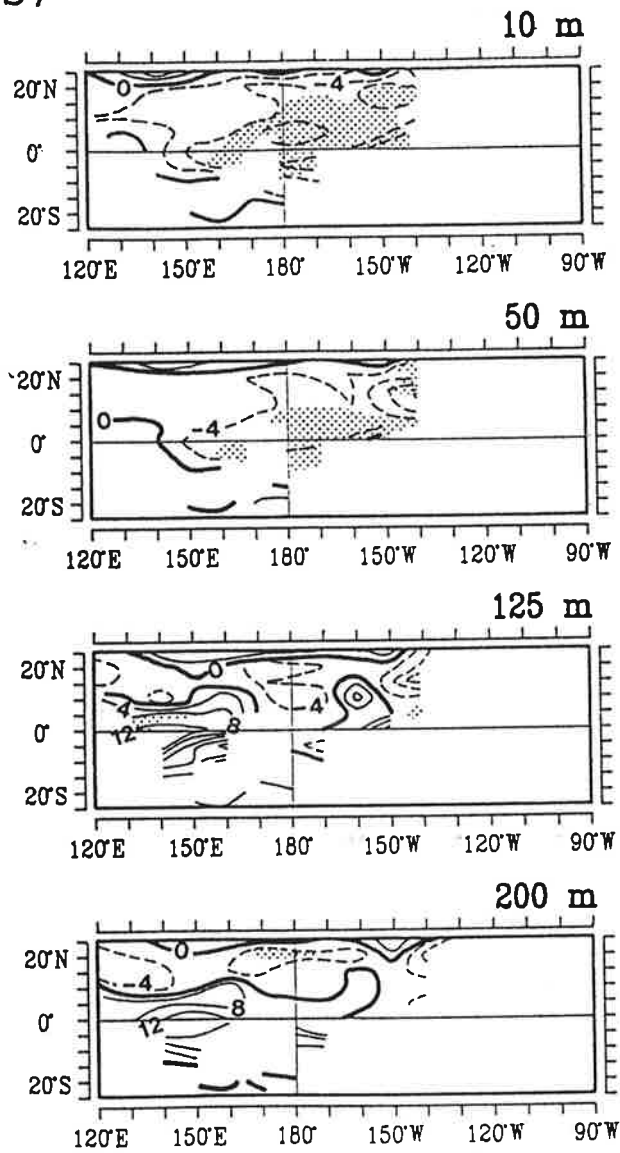
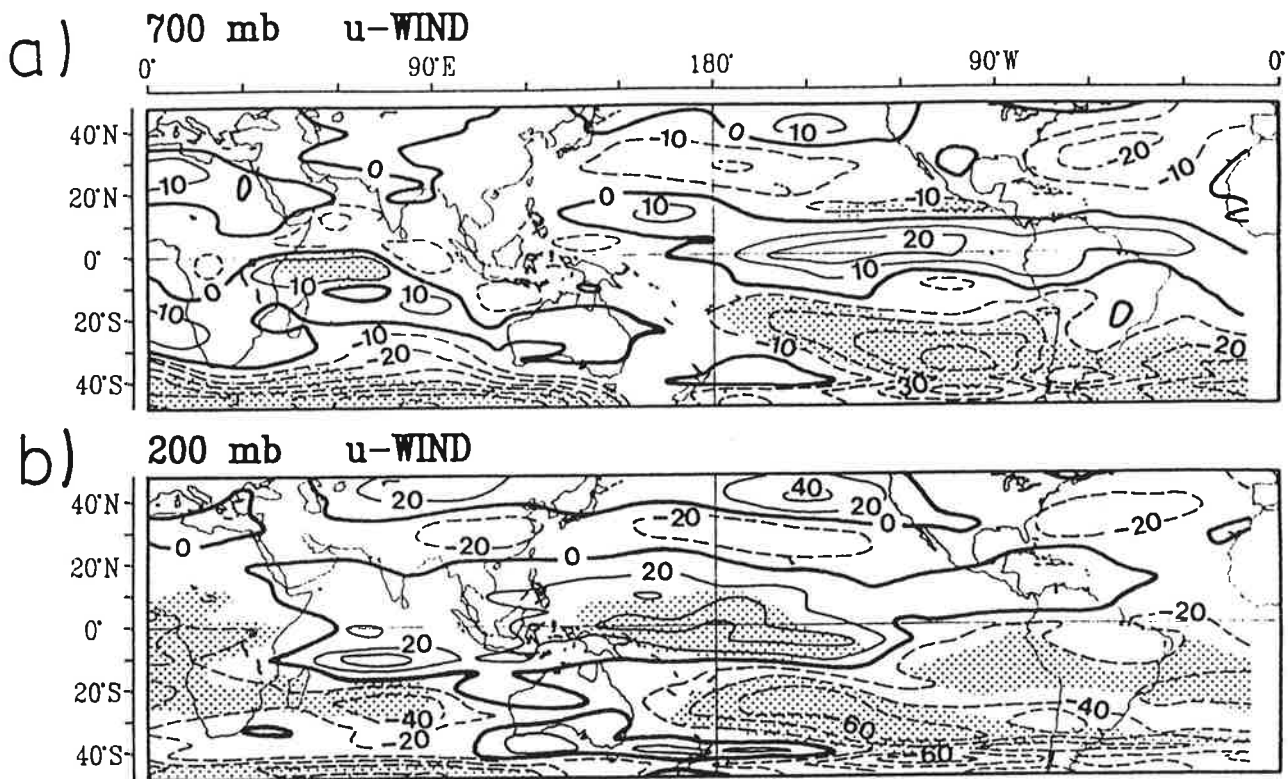


Figure 13: POP pattern of Mode 5 for a) sea surface temperature (in °C) and b) Pacific subsurface temperature. Shaded areas indicate explained variance larger than 10%.



**Figure 14:** POP pattern of Mode 5 for a) 700-mb zonal wind (in m/s) and b) 200-mb zonal wind (in m/s). Shaded areas indicate explained variance larger than 10%.

the South Indian Ocean and South Atlantic, and a double jet structure in the western South Pacific with minimum values along 40°S. Fig.2e indicates that this mean circulation pattern changed very rapidly during 1975/76, with an anomalous weak jet over the southern Indian Ocean and the South Atlantic and an anomalous weak double jet structure over the western part of the South Pacific during the first half of the time period, and an anomalous strong jet and strong double jet structure during the second half of the period.

No air-sea process of the type summarized in section 3 can be identified for Mode 5. It is not clear at this stage, how and why the global-scale SST anomalies (Fig.13a) and the changes in the Southern Hemisphere circulation (Fig.14a, b) are related to each other.

#### 5.4 THE JOINT OSCILLATORY NORMAL MODE: Mode 6

As mentioned in section 2, a complex POP is only defined to an arbitrary complex factor  $e^{i\theta}$ . I will show later that the complex Mode 6 describes the Southern Oscillation phenomenon. To simplify the interpretation,  $\theta$  is chosen so that the imaginary part of the POP coefficient time series is maximally correlated (0.72) with the conventional Southern Oscillation Index (pressure

difference between Tahiti and Darwin). Therefore, the imaginary part of the POP, noted as  $P^{im}$ , describes the anomalies associated with the cold extreme of the ENSO phenomenon, and the real part, noted as  $P^{re}$ , corresponds to the intervening phase, i.e., conditions which appear about one year before a warm extreme.

#### a) ATMOSPHERIC AND OCEANIC FEATURES OF THE MODE 6

For SLP, the evolution from a cold extreme to a warm extreme is described by an eastward migration of the negative anomalies from the Indian Ocean and the West Pacific during a cold extreme ( $P^{im}$  in Fig.15a), into the West and Central Pacific during the intervening phase ( $P^{re}$  in Fig.16a), and finally into the Central and East Pacific during the warm extreme ( $-P^{im}$ ). Associated with this evolution an eastward migration of low level westerly wind anomalies is observed with anomalous westerlies propagating from the Indian Ocean in Fig.15b into the West Pacific in Fig.16b and into the Central Pacific. At 200-mb the conditions during the extreme phase (Fig.15c) are well known with strong anomalous westerlies over the Central Pacific on the Equator and the anomalous easterlies in the subtropical Pacific, whereas during the intervening phase (Fig.16c) strong westerlies are found over most of the tropical oceans. It seems that the migration feature is more pronounced at the lower than at higher level.

The maximum of variance explained by this cyclic evolution is shown by the shaded areas in Fig.15 and Fig.16. For SLP, the signal in the Southern Hemisphere is stronger than that in the Northern Hemisphere. For the wind, the signal is strong in the West and Central Pacific at 700-mb, and over the Central Pacific and the subtropical South and North Pacific at 200-mb. The explained variance for both the low and high level parameters shows maximal values up to about 35% along the Equator and decreases rapidly poleward, especially for SLP and the 700-mb zonal winds.

In the ocean, there is little evidence of migration in the SST (Fig.17a, 18a). But in terms of the ocean temperature and sea level (Fig.17b,c and Fig. 18b,c), propagation of anomalies is clearly presented. The sea level anomalies during a cold event ( $P^{im}$  in Fig. 17c) are associated with large positive values over the West Pacific, which has a larger extension north of the Equator than south of the Equator. On the Equator there is a minimum of positive anomalies in the west part of the Pacific and a tongue of negative anomalies in the Central and East Pacific. In the intervening stage ( $P^{re}$  in

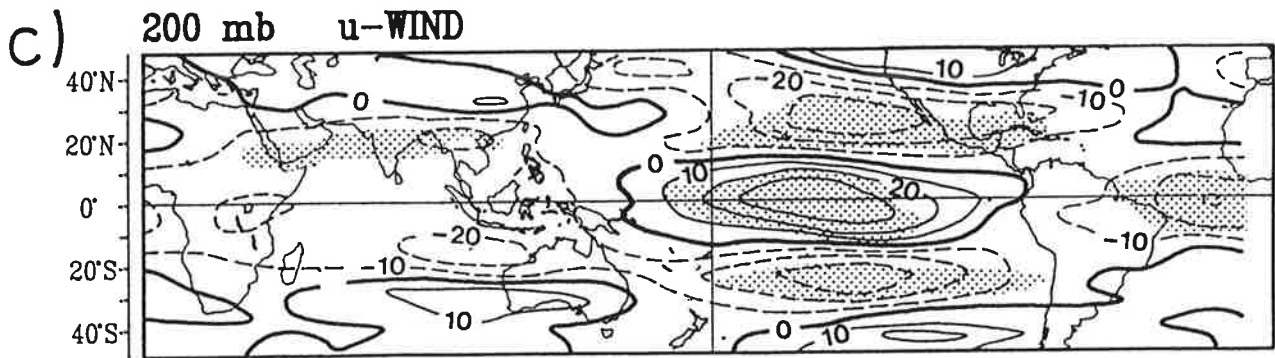
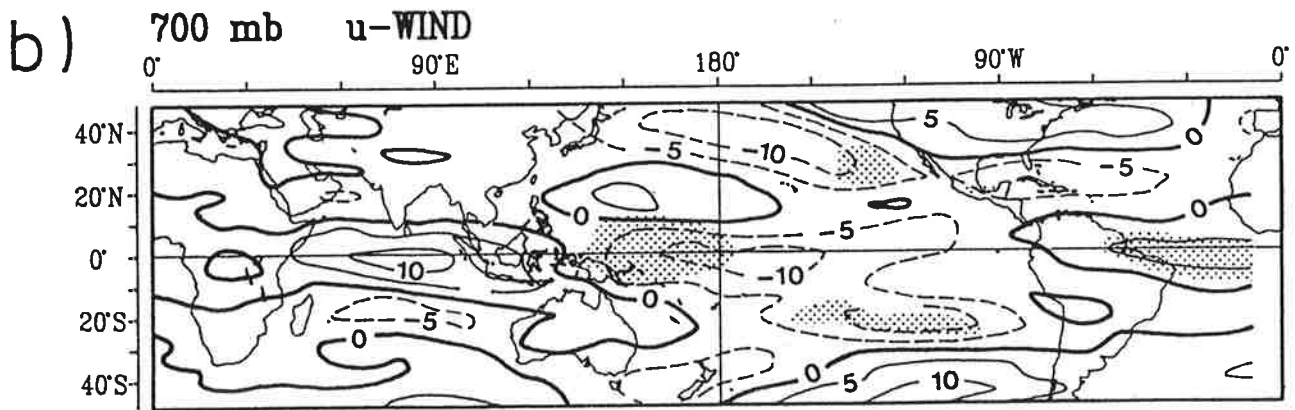
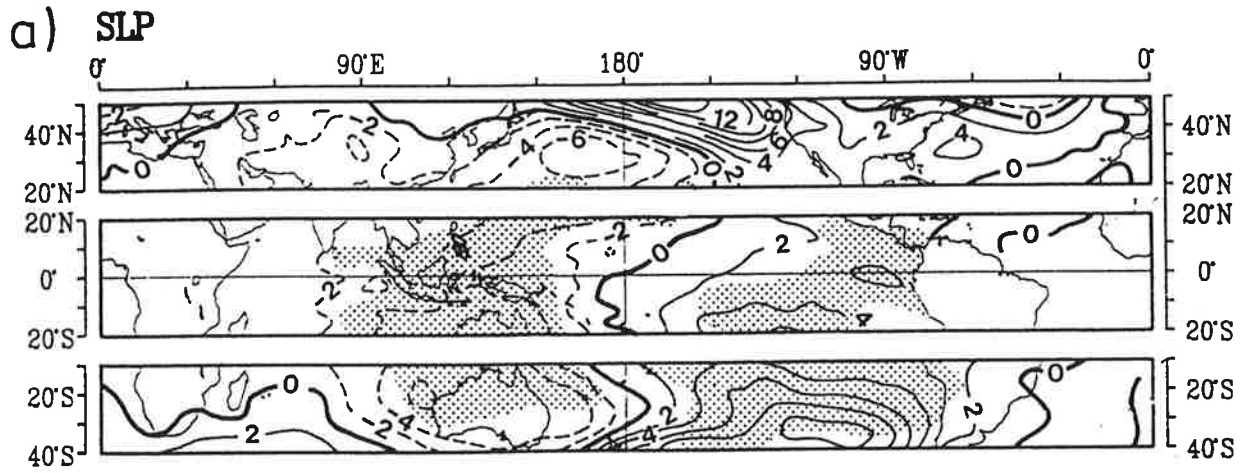
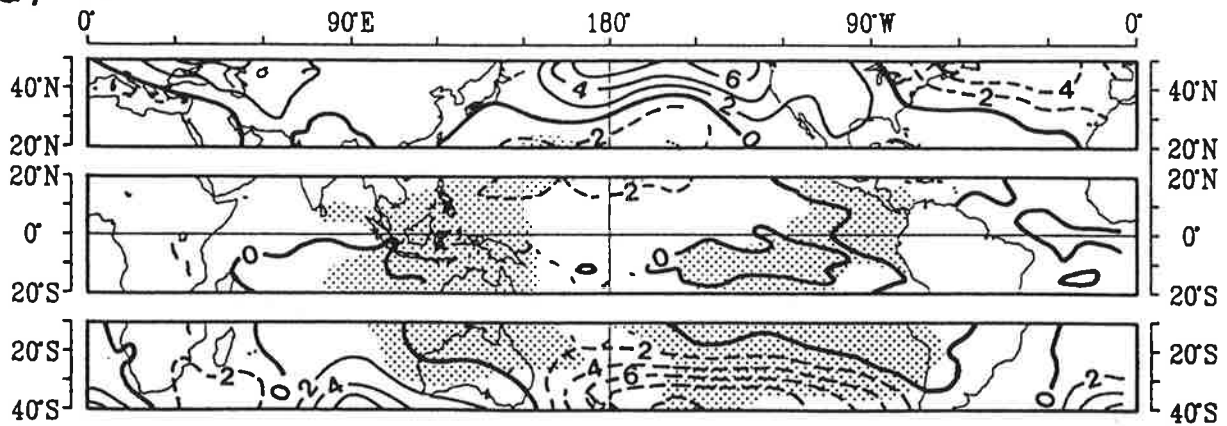
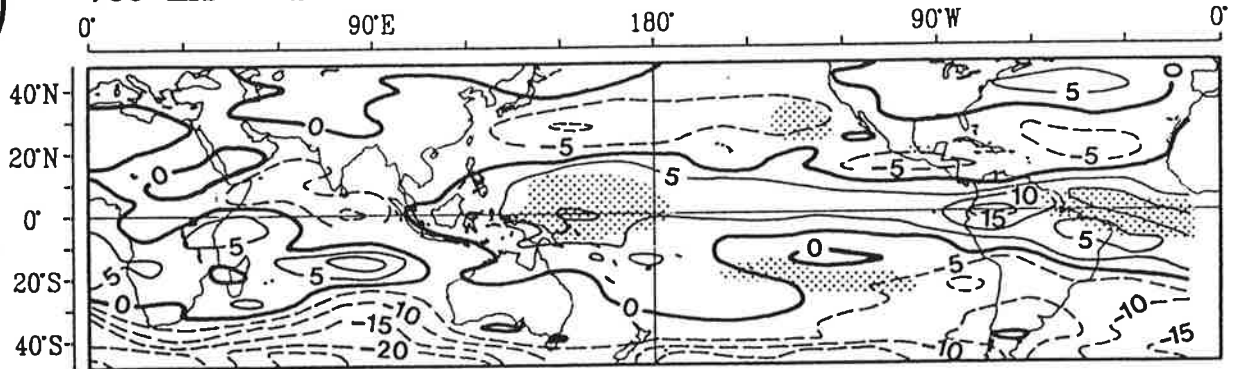


Figure 15: POP pattern of the imaginary part of Mode 6 for a) sea level pressure (in mb), b) 700-mb zonal wind (in m/s) and c) 200-mb zonal wind (in m/s). Shaded areas indicate explained variance larger than 15%.

a) SLP



b) 700 mb u-WIND



c) 200 mb u-WIND

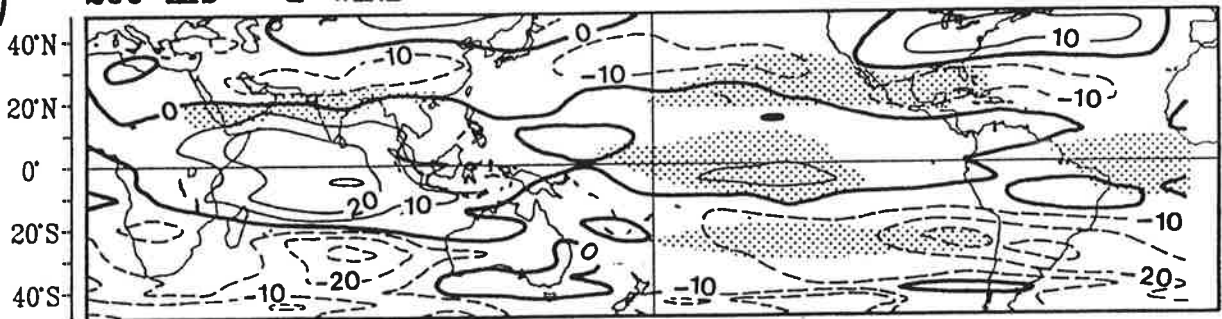


Figure 16: POP pattern of the real part of Mode 6 for a) sea level pressure (in mb), b) 700-mb zonal wind (in m/s) and c) 200-mb zonal wind (in m/s). Shaded areas indicate explained variance larger than 15%.

Fig.18c), the positive sea level anomalies have now moved into the West and Central Pacific. The same evolution with even more detailed distribution is shown for the Pacific Ocean temperature in Fig.17b and Fig.18b. The largest temperature anomalies are reached during a cold extreme in the West Pacific at about 5°S at 200 meters deep, and at about 5°N-10°N at 125 meters deep. They then migrate equatorward and are located on the Equator in the west Central Pacific during the intervening stage.

Explained variances larger than 30% for sea level and larger than 30% for temperature are shown by shaded areas in Fig.17 and 18. As in the case of atmospheric parameters, maximal values are located in the equatorial regions.

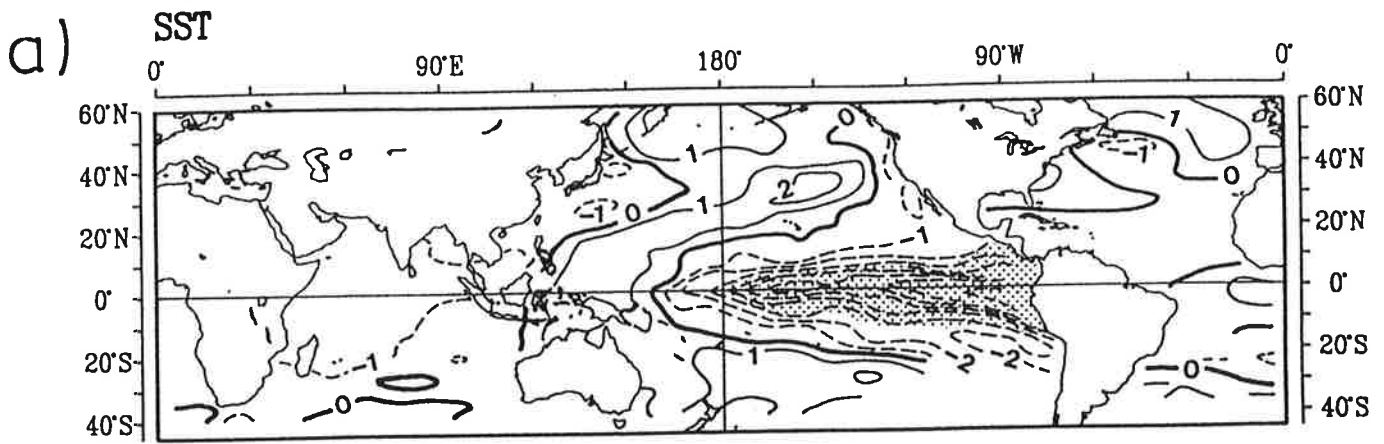
#### b) AIR-SEA INTERACTIONS INVOLVED IN MODE 6

The fact that ENSO appears as an oscillatory normal mode of the atmosphere-ocean system is consistent with previous studies. The well defined mode in the Tropical Pacific, suggested as being a delayed oscillation mode (Suarez and Schopf, 1988), and also found in an ocean GCM (Latif and Flügel, 1991) displays similar sea level evolution to that given by the oscillatory Mode 6: The positive sea level anomalies located off the Equator in the West Pacific and the tongue of negative sea level anomalies in the equatorial central and eastern Pacific in  $P^{im}$  (Fig.17c) resemble the sea level anomalies associated with westward propagating Rossby waves and eastward propagating Kelvin waves; and the positive anomalies in  $P^{re}$  (Fig.18c) seem to have been reflected at the western boundary and appear as a Kelvin wave signal centered along the Equator. Also the atmospheric part of the evolution is consistent with that shown first by Barnett (1985, 1988). The new suggestion of this paper is that the oceanic mode is probably tied to the propagating features of the atmospheric anomalies.

The relation between the atmospheric and the oceanic propagating features appears as the following. The sea level anomalies in both the extreme phase and the intervening phase are likely to be produced by anomalous atmospheric conditions: the sea level pattern in Fig.17c by easterly anomalies over the tropical Pacific (Fig.15b), and the sea level pattern in Fig. 18c by westerly anomalies over the West Pacific (Fig.16b). It is speculated that the cyclic evolution of oceanic anomalies can be interpreted as the oceanic response to the eastward movement of the low level zonal wind anomalies.

Now what is the reason for the cyclic evolution of the wind anomalies? As





b) SUBSURFACE TEMPERATURE

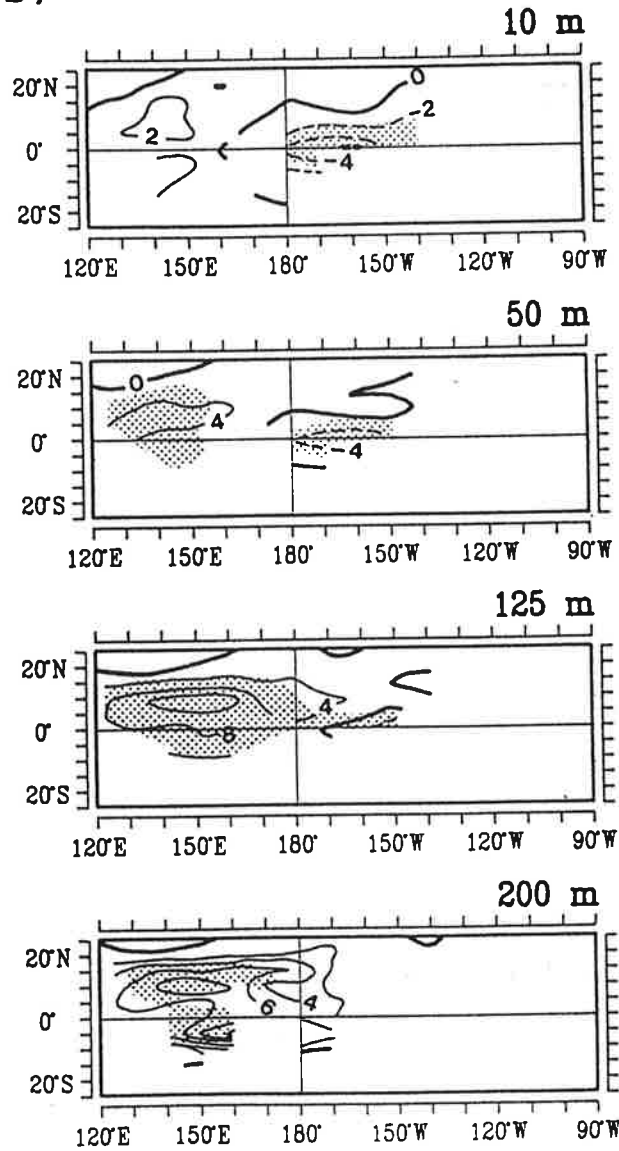
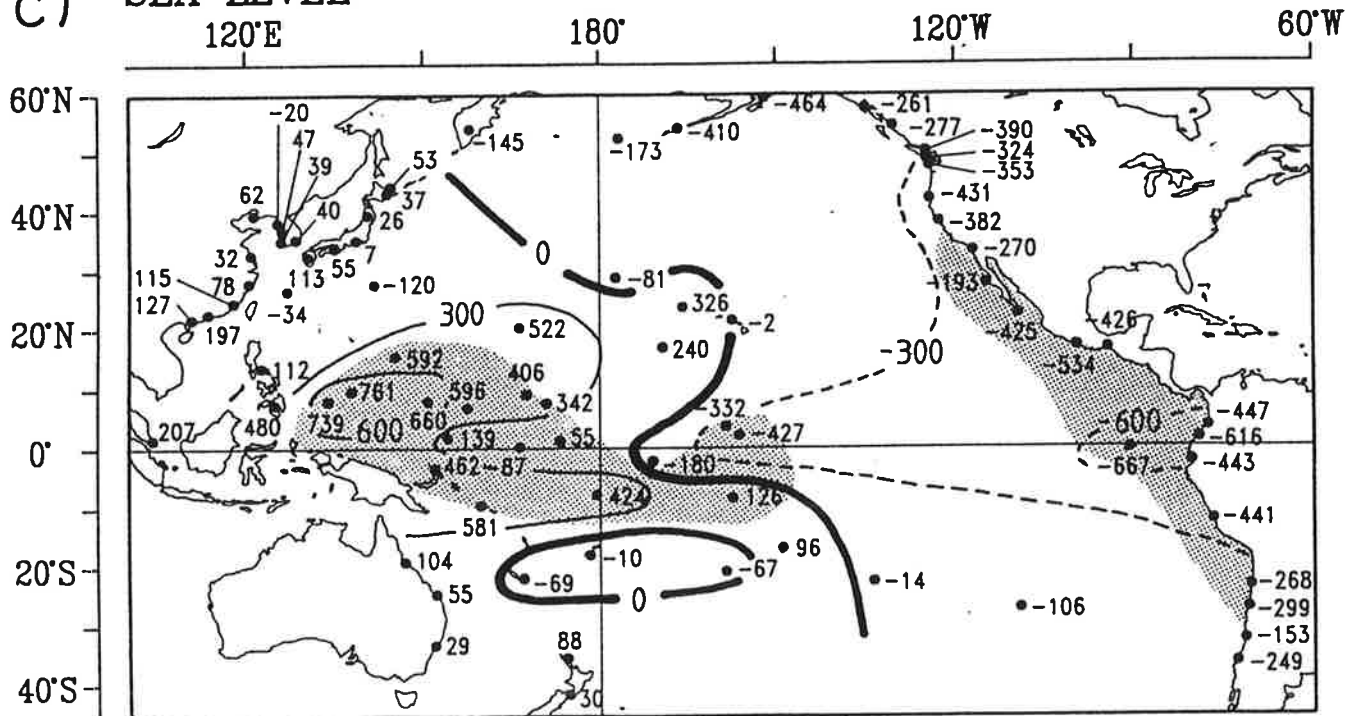
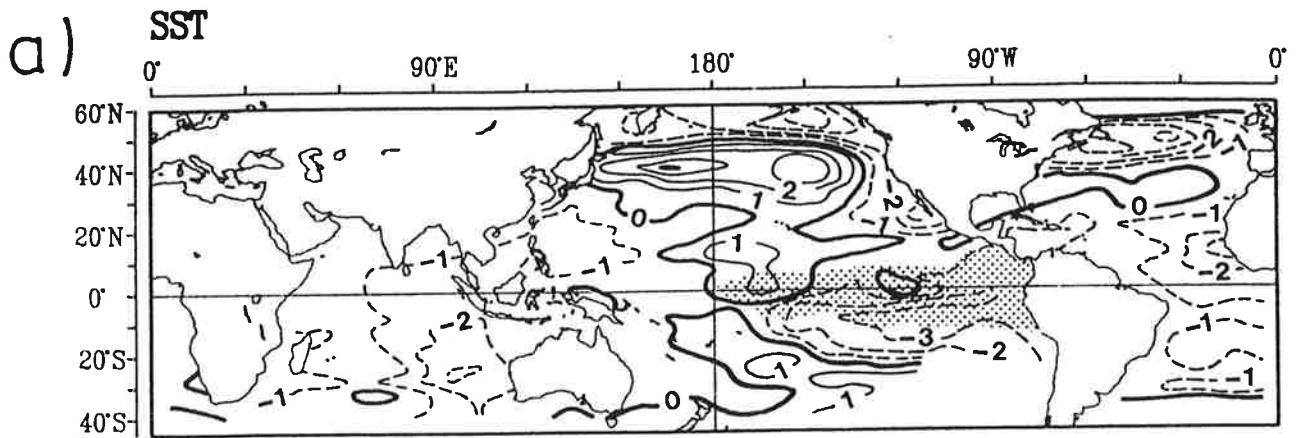


Figure 17: POP pattern of the imaginary part of Mode 6 for a) SST (in  $^{\circ}\text{C}$ ), b) the Pacific sub-surface temperature (in  $^{\circ}\text{C}$ ), and c) Pacific sea level (in mm). Shaded areas indicate explained variance larger than 30%.

# c) SEA LEVEL



Continue of Figure 17



b) SUBSURFACE TEMPERATURE

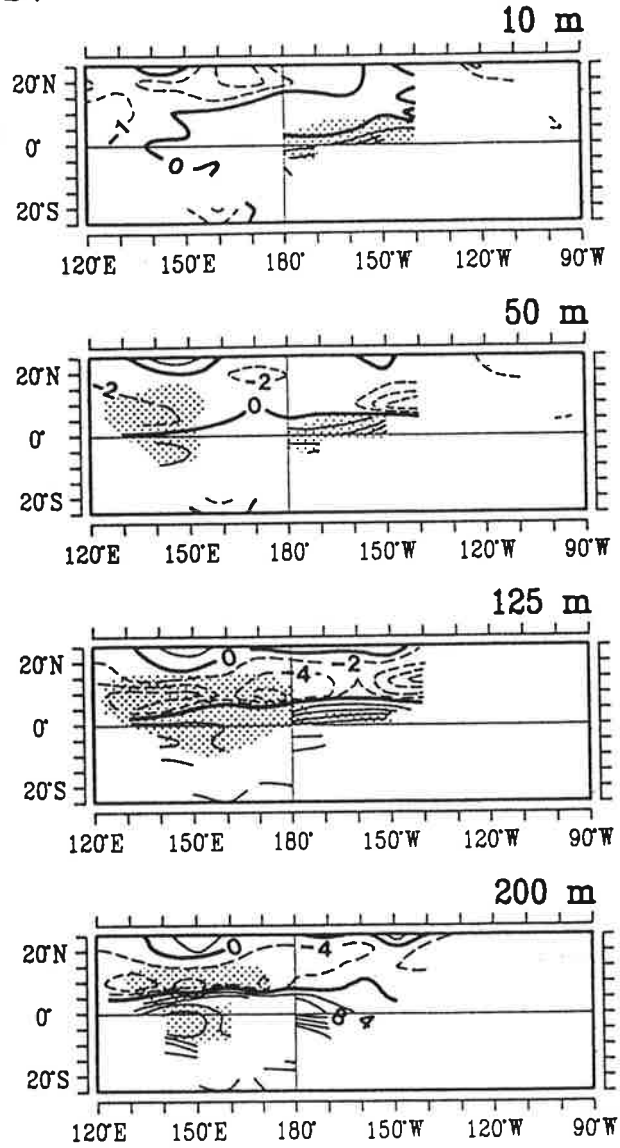
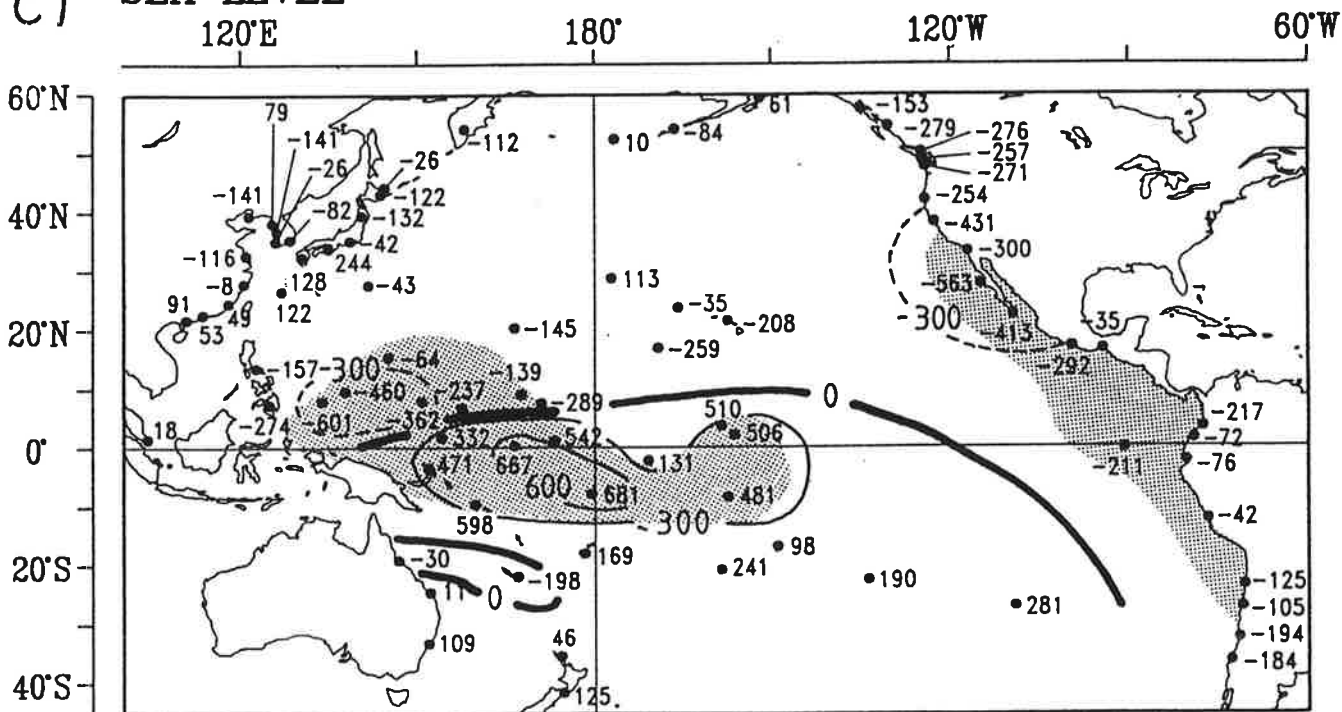


**Figure 18:** POP pattern of the real part of Mode 6 for a) SST (in °C), b) the Pacific sub-surface temperature (in °C), and c) Pacific sea level (in mm). Shaded areas indicate explained variance larger than 30%.

c) SEA LEVEL



Continue of Figure 18

discussed in section 3, SST is the only forcing for the overlying atmosphere in this context. During the extreme phase, a comparison between SST in Fig.17a and wind patterns in Fig.15 indicates that atmospheric anomalies appear as response to the heating anomalies with anomalous convection (an expression of low level convergence and upper level divergence) sitting over the warm water in the West during the cold phase and in the East during the warm phase. But during the intervening phase, no notable SST anomalies can be related to the anomalous westerlies over the West Pacific. This indicates that the movement of the wind anomalies is not forced by the SST.

## 6. CONCLUSIONS

### a) ESTIMATED NORMAL MODES

A possibility of estimating normal modes of a complex system from data is presented in this paper. Although the analogy between the estimated normal modes (POPs) and the theoretical normal modes has been demonstrated by Storch et al. (1991) in an example of atmospheric baroclinic waves, our results show further evidences of this analogy for normal modes on longer time scales and in a more complex system. Because of the complexity of the coupled atmosphere-ocean system, the POP analysis seems to be the only techniques, at this stage, for studying the normal modes of this system.

A disadvantage in estimating normal modes from data is that the physical processes involved in these modes cannot be determined by the analysis procedure. The processes in the normal modes found are suggested objectively by using information summarized in section 3. More data and other theoretical studies are needed to prove the results.

### b) MULTIVARIATE SPECTRAL ANALYSIS

The agreement between the spectrum given by an eigenvalue or derived from the corresponding POP coefficient time series demonstrates clearly the ability of the POP analysis to pick out the spatially coherent modes together with their spectral features summarized by the eigenvalues.

### c) AIR-SEA PROCESSES ON DIFFERENT TIME SCALES

As mentioned in section 4, the modes found in this study are probably the *joint* normal modes of the coupled atmosphere-ocean system. The results

indicate that different air-sea processes are involved in these modes. Whereas the atmosphere is responsible for the modes which vary on month to month time scales, the role of the ocean becomes more important for the modes which vary on much longer time scales.

On month-to-month time scales, the large-scale oceanic anomalies could be understood as being forced by large-scale extratropical atmospheric anomalies. The SST anomalies were mainly caused by anomalous warm and cold air advection and the sea level anomalies appeared to be produced by the inverse barometric effect.

On decadal time scales, one air-sea process described in section 5.2 seemed to have its origin in the tropics. This mode shows large-scale SST anomalies in all three tropical oceans and organized convection over the tropical West Pacific. A further investigation of the patterns allows us to speculate that this tropical variation could induce changes in the extratropical tropospheric circulation and these might cause changes in the subtropical and subpolar gyres in the North Pacific.

On ENSO time scales, cyclic oceanic anomalies seemed to be tied to the eastward propagation of the atmospheric anomalies. However, the results indicate that oceanic forcing in terms of SST is present only during the extreme phase of ENSO, but not during the intervening phase.

## ACKNOWLEDGEMENTS

I would like to express my gratitude to Klaus Hasselmann for his inspiration to this topic. I also like to thank Dennis Moore and Klaus Wyrski for their suggestions about oceanic anomalies. Many thanks to Grant Branstator, Hans von Storch, Mojib Latif, Ute Luksch, Nanne Weber, Ernst Maier-Reimer, Jörg-Olaf Wolff, Eduardo Zorita and Gerd Bürger for many fruitful discussions. Thanks also to M. Grunert and D. Lewandowsky for preparing the diagrams, to P.B. Wright for editing the English, and to Jutta Bernlöhr and Heike Schriever for typing the manuscript.

## REFERENCES:

- Barnett, T.P., 1985:** Variations in near-global sea level pressure. - *J. Atmos. Sci.*, **42**, 478-501.
- Barnett, T.P., 1988:** Variations in near-global sea level pressure: another view. - *J. Climate*, **1**, 222-230.
- Bjerknes, J., 1962:** Synoptic survey of the interaction between sea and atmosphere in the North Atlantic. - *Geofysiske publikasjoner*, **24**, 116-145.
- Egger, J., 1977:** On the linear theory of the atmospheric response to sea surface temperature anomalies. - *J. Atmos. Sci.* **34**, 603-614.
- Flohn, H.; A. Kapala; H.-R. Knoche and H. Mächel, 1990:** Recent changes of tropical water and energy budget and of midlatitude circulations. - *Climate Dynamics* **4**: 237-252.
- Hasselmann, K., 1988:** PIPs and POPs: the reduction of complex dynamical systems using Principal Interaction and Oscillation Patterns. - *J. Geophys. Res.*, **93**, 11015-11021.
- Gill, A. E., 1980:** Some simple solutions for heat-induced tropical circulation. - *Quart. J. R. Met. Soc.*, **106**, 447-462.
- Gill, A.E. and P.P. Niiler, 1973:** The theory of seasonal variability in the ocean. - *Deep-sea Res.* **20**, 141-177.
- Latif, M and M. Flügel, 1991:** An investigation of short-range climate predictability in the tropical Pacific. - *J. Geophys. Res.* **96**, 2661-2673.
- Luksch, U. and H.v. Storch, 1992:** Modelling the low-frequency sea surface temperature variability in the North Pacific. - accepted by *J. Climate*.
- Qiu, B. and T. M. Joyce, 1991:** Interannual variability in the mid- and low-latitude western North Pacific. - accepted by *J. Phys. Oceanogr.*
- Simmons, A.J., J.M., Wallace and G.W. Branstator, 1983:** Barotropic wave propagation and instability, and atmospheric teleconnection patterns. - *J. Atmos. Sci.* **40**, 1363-1392.



**Storch, H. v., T. Bruns, I. Fischer-Bruns and K.H. Hasselmann, 1988:** Principal Oscillation Pattern analysis of the 30 to 60 day oscillation in a GCM. - J. Geophys. Res., **93**, 11022-11036.

**Storch, H. v.; G. Bürger; R. Schnur and J. Xu, 1991:** POP art. - Ed. Latif: Strategies for future climate research. Max-Planck Institut für Meteorologie, Bundesstrasse 55, D-2000 Hamburg 13, Germany.

**Suarez, M. and P.S. Schopf, 1988:** A delayed action oscillator for ENSO. - J. Atmos. Sci., **45**, 3282-3287.

**van Loon, H., 1972:** Wind in the Southern Hemisphere. Meteorology of the Southern Hemisphere, Ed. C.W. Newton, Meteor. Monogr. **35**, Amer Meteor. Soc. **35**, 87-100.

**Wallace, J.M. and Gutzler, D.S., 1981:** Teleconnections in the geopotential height field during the Northern Hemisphere winter. - Min. Wea. Rev., **109**, 784-812.

**Webster, P. 1981:** Mechanism determining the atmosphere response to sea surface temperature anomalies. - J. Atmos. Sci., **38**, 554-571.

**Woodruff, S. D; R. J. Sultz; R. L. Jenne and P. M. Steurer, 1987:** A comprehensive ocean - atmosphere data set. - Bull. Amer. Met. Soc. **68**, 1239-1250.

**Wright, P.B., Wallace, J.M., Mitchell, T.P. and Deser., C., 1988:** Correlation structure of the El Niño / Southern Oscillation Phenomenon. J. Climate, **1**, 609-625.

**Wyrli, K; K. Constantine; B. J. Kilonsky; G. Mitchum; B. Miyamoto; T. Murphy; S. Nakahara and P. Caldwell, 1988:** The Pacific Island sea level network. - JIMAR Contrib. **88-0137**, Data Rep. **002**, Univ. of Hawaii, Honolulu.

**Xu, J. and H.v. Storch, 1990:** Predicting the state of the Southern Oscillation Using Principal Oscillation Pattern Analysis. - J. Climate, **3**, 1316-1329.

**Xu, J., 1991:** On the relationship between the stratospheric QBO and the tropospheric SO. - J. Atmos. Sci., in press.

**Zorita E., V. Kharin. and H.v. Storch, 1992:** The atmospheric circulation and sea surface temperature in the North Atlantic area in winter: their interaction and relevance for Iberian precipitation. - accepted by J. Climate, also MPI report no.54., Bundesstrasse 55, D-2000 Hamburg, Germany.